

# Supplementary Materials for

## **Structural Basis for Protein anti-Aggregation Activity of the Trigger Factor Chaperone**

Tomohide Saio, Xiao Guan, Paolo Rossi, Anastassios Economou, Charalampos G. Kalodimos

Corresponding author. E-mail: [babis@rutgers.edu](mailto:babis@rutgers.edu)

### **The PDF file includes:**

Figs. S1 to S27

Table S1

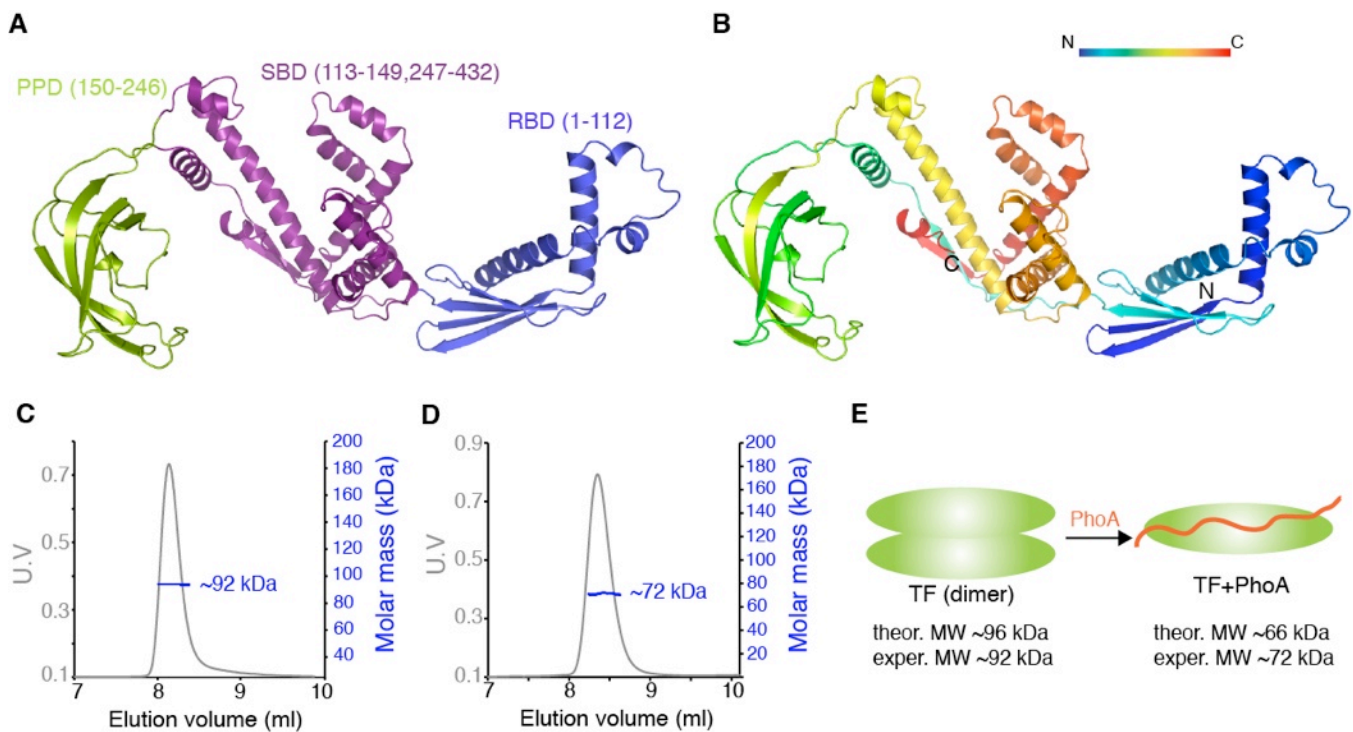


**Fig. S1. Domain architecture and oligomerization state of TF.** (A) Structure of *E. coli* TF (PDB ID 1W26). The residue boundaries for each one of the three domains are shown in parentheses. SBD is discontinuous and is formed primarily by the C-terminal domain. (B) The backbone of TF is colored using a gradient color scheme from the N terminus (blue) to the C terminus (red). (C) MALS of unliganded TF shows that the protein forms a dimer in solution. (D) MALS of TF in complex with the first 141 residues of PhoA containing TF-binding sites *a*, *b*, and *c* (PhoA<sup>a-c</sup>) shows that TF binds to PhoA as a monomer. TF is also a monomer in its complex with PhoA<sup>d-e</sup> and PhoA<sup>f-g</sup>, as well as with MBP and OmpA. (E) Schematic showing the monomerization undergone by TF upon substrate (PhoA) binding.

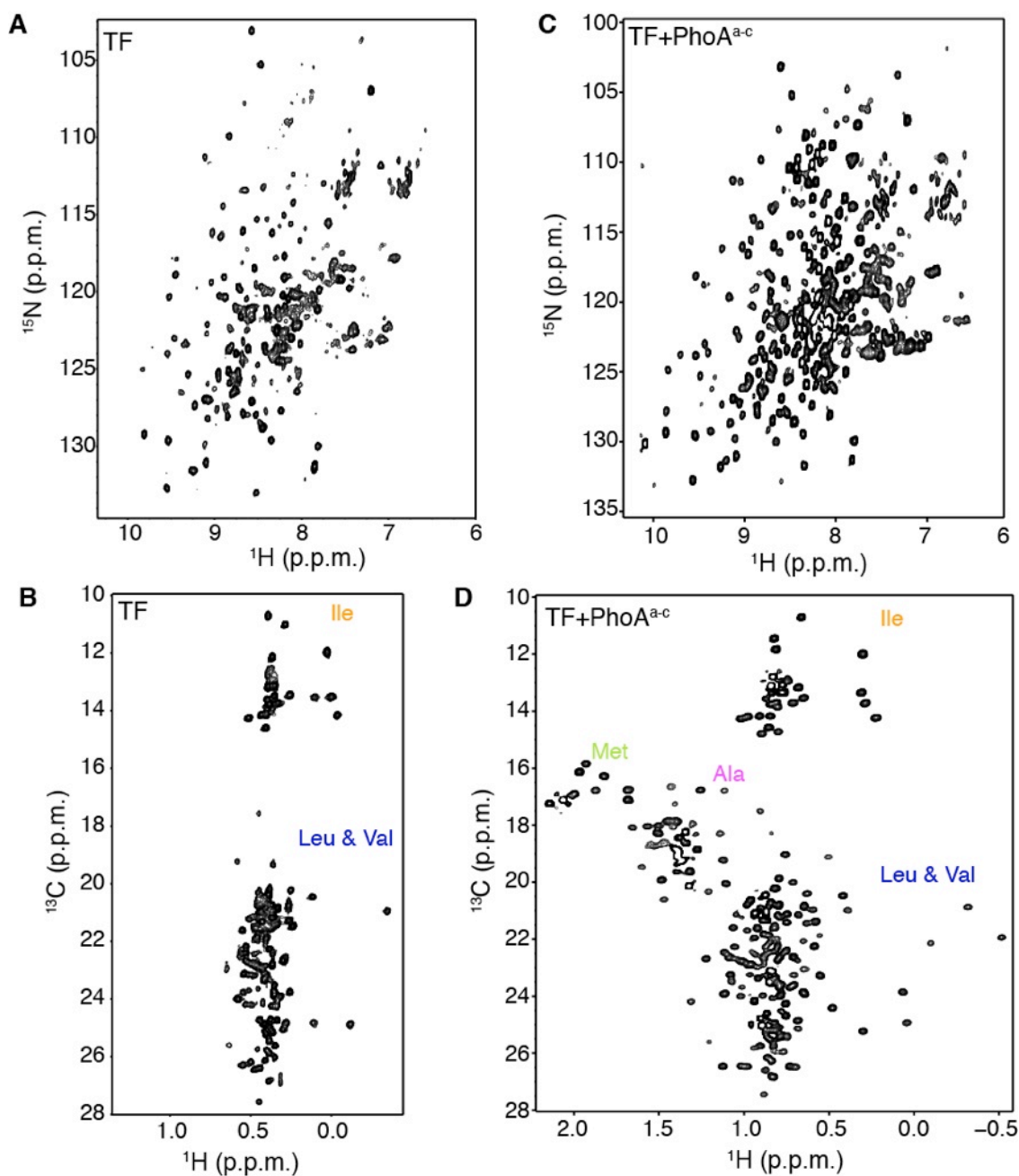


**Fig. S2. NMR spectra of unliganded TF and in complex with PhoA.** (A)  $^1\text{H}$ - $^{15}\text{N}$  TROSY HSQC of [ $\text{U}$ - $^2\text{H}$ ,  $^{15}\text{N}$ ]-labeled and (B)  $^1\text{H}$ - $^{13}\text{C}$  methyl HMQC spectra of [ $\text{U}$ - $^2\text{H}$ ; Ile- $\delta 1$ - $^{13}\text{CH}_3$ ; Leu, Val- $^{13}\text{CH}_3$ / $^{13}\text{CH}_3$ ]-labeled dimeric TF (unliganded). Analysis of the spectra shows that several resonances are broadened beyond detection, presumably because of slow motions at the dimeric interface (see fig. S19). (C)  $^1\text{H}$ - $^{15}\text{N}$  TROSY HSQC of [ $\text{U}$ - $^2\text{H}$ ,  $^{15}\text{N}$ ]-labeled and (D)  $^1\text{H}$ - $^{13}\text{C}$  methyl HMQC spectra of [ $\text{U}$ - $^2\text{H}$ ; Ala- $^{13}\text{CH}_3$ ; Met- $^{13}\text{CH}_3$ ; Ile- $\delta 1$ - $^{13}\text{CH}_3$ ; Leu, Val- $^{13}\text{CH}_3$ / $^{13}\text{CH}_3$ ]-labeled TF in complex with PhoA<sup>a-c</sup>. Analysis of the spectra indicates that all of the expected resonances are present. The dispersion and sensitivity of these spectra are excellent. Both TF and PhoA<sup>a-c</sup> are labeled.

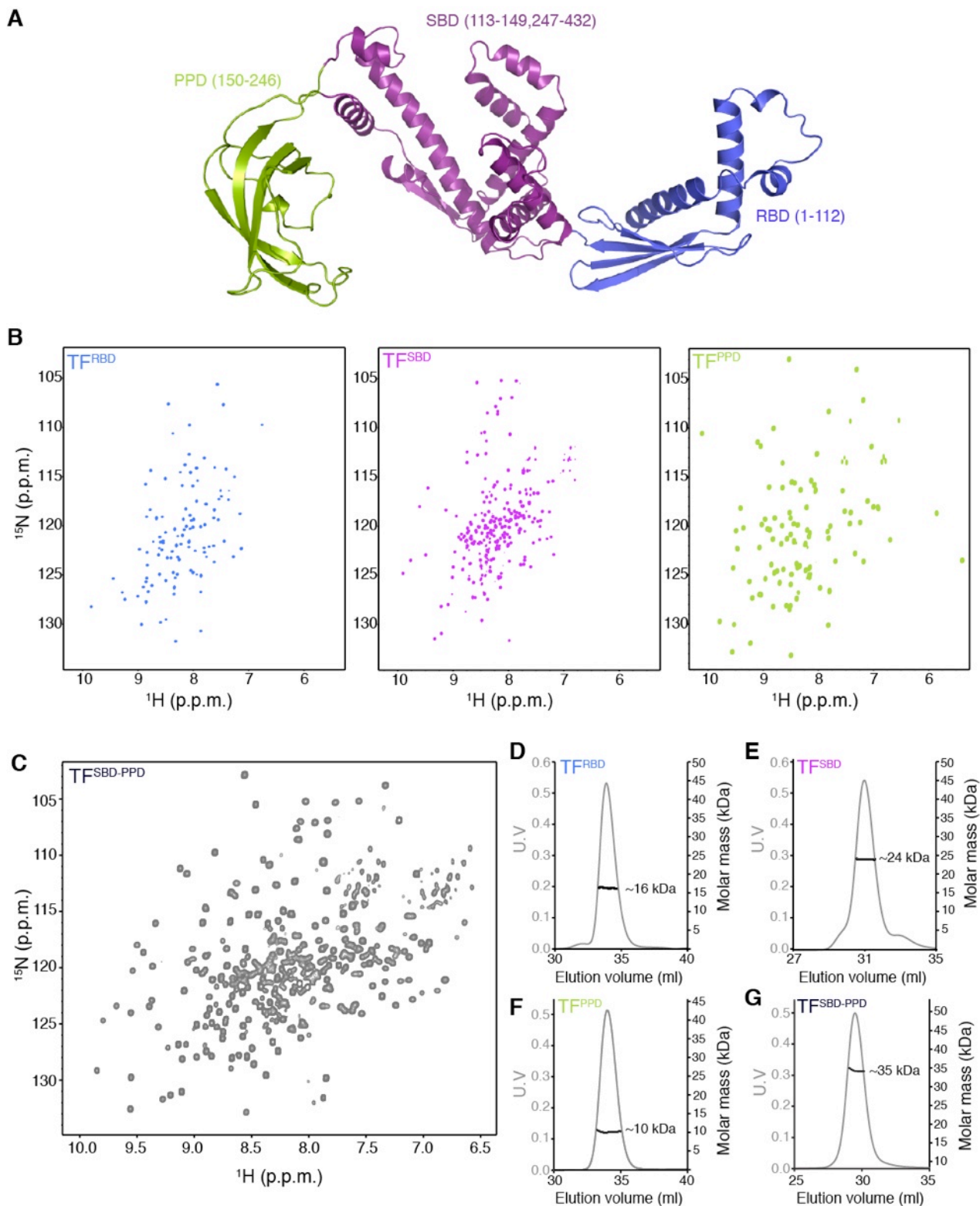


**Fig. S3. NMR spectra of TF and its isolated domains.** (A) Structure of TF. (B)  $^1\text{H}$ - $^{15}\text{N}$  HSQC spectra of the individual domains of TF indicate that they retain their proper fold when in isolation. (C)  $^1\text{H}$ - $^{15}\text{N}$  TROSY HSQC spectrum of  $[\text{U}_2\text{-}^2\text{H}, ^{15}\text{N}]$ -labeled  $\text{TF}^{\text{SBD-PPD}}$ , a TF construct that consists of the SBD and PPD domains (residues 113-432), the two domains with chaperone activity. (D to G), MALS of isolated TF domains RBD (in D), SBD (in E), PPD (in F), and SBD-PPD (in G) show that all of these domains or fragments are monomeric in solution.

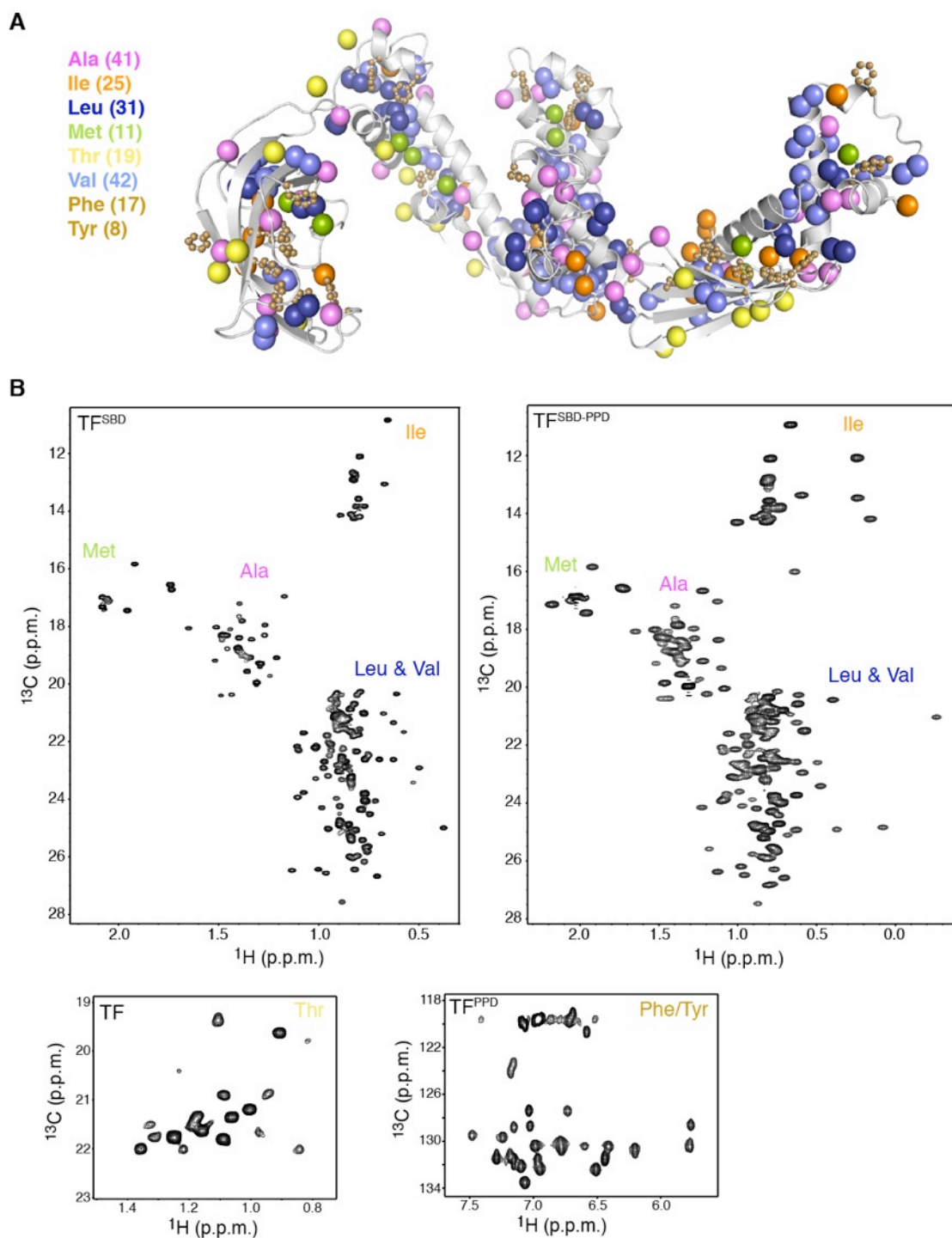


**Fig. S4. Side chain NMR spectra of TF.** (A) TF is enriched in hydrophobic residues, such as methyl-bearing (Ala, Ile, Leu, Met, Thr, and Val) and aromatic residues (Phe and Tyr). The numbers in parentheses indicate the number of the corresponding residues in TF (per subunit). (B)  $^1\text{H}$ - $^{13}\text{C}$  methyl HMQC spectra of [ $\text{U}\text{-}^2\text{H}$ ; Ala- $^{13}\text{CH}_3$ ; Met- $^{13}\text{CH}_3$ ; Ile- $\delta 1$ - $^{13}\text{CH}_3$ ; Leu,Val- $^{13}\text{CH}_3/^{13}\text{CH}_3$ ]-labeled TF<sup>SBD</sup> and TF<sup>SBD-PPD</sup>, and of [ $\text{U}\text{-}^2\text{H}$ ; Thr- $^{13}\text{CH}_3$ ]-labeled dimeric TF, and aromatic  $^1\text{H}$ - $^{13}\text{C}$  HSQC spectra of TF<sup>PPD</sup>, a domain enriched with aromatic residues.

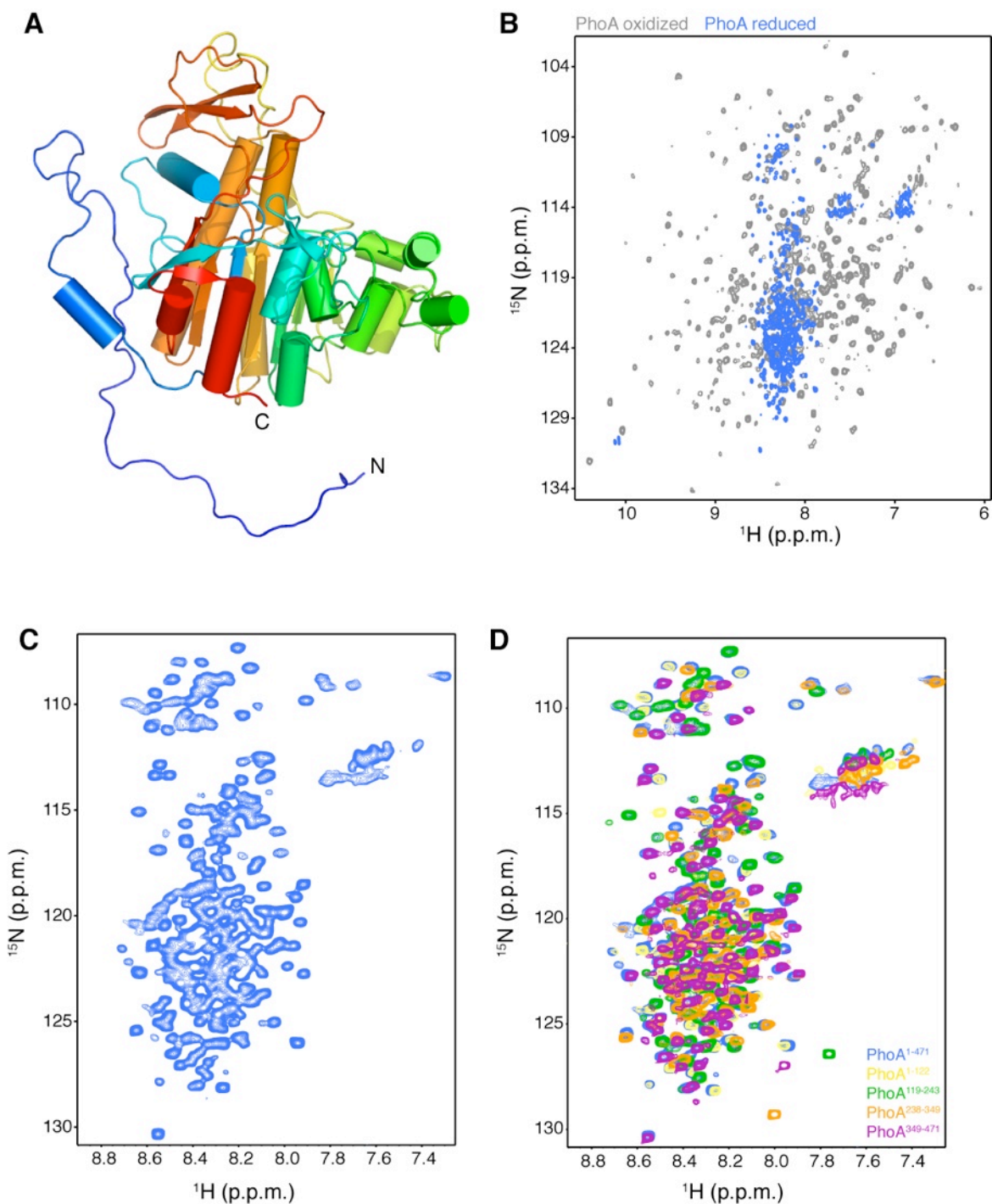


**Fig. S5. NMR analysis of PhoA.** (A) Crystal structure of PhoA under oxidizing conditions (PDB ID 1Y6V). Folded PhoA forms a dimer but only one subunit is shown here. Only the mature portion of PhoA was solved crystallographically (residues 23-471). The signal sequence (residues 1-22) was modeled as an unstructured N terminal sequence in the crystal structure and is depicted here. The structure is colored using a gradient color from the N terminus (blue) to the C terminus (red). (B)  $^1\text{H}$ - $^{15}\text{N}$  HSQC spectra of PhoA under oxidizing (grey) and reducing conditions (blue). The NMR spectra clearly show that oxidized PhoA is folded whereas reduced PhoA is unfolded. (C) An expanded view of the  $^1\text{H}$ - $^{15}\text{N}$  HSQC spectrum of reduced, unfolded PhoA. (D) Overlaid  $^1\text{H}$ - $^{15}\text{N}$  HSQC spectra of full-length PhoA and select PhoA fragments that span the entire sequence of PhoA (aa 1-471). The spectra of the fragments are exact subsets of the full-length PhoA spectrum. The excellent resonance correspondence is expected since all of the fragments and the full-length PhoA are unfolded. Resonance assignment obtained for the various fragments was transferred to the full-length PhoA using 3D NMR spectra.

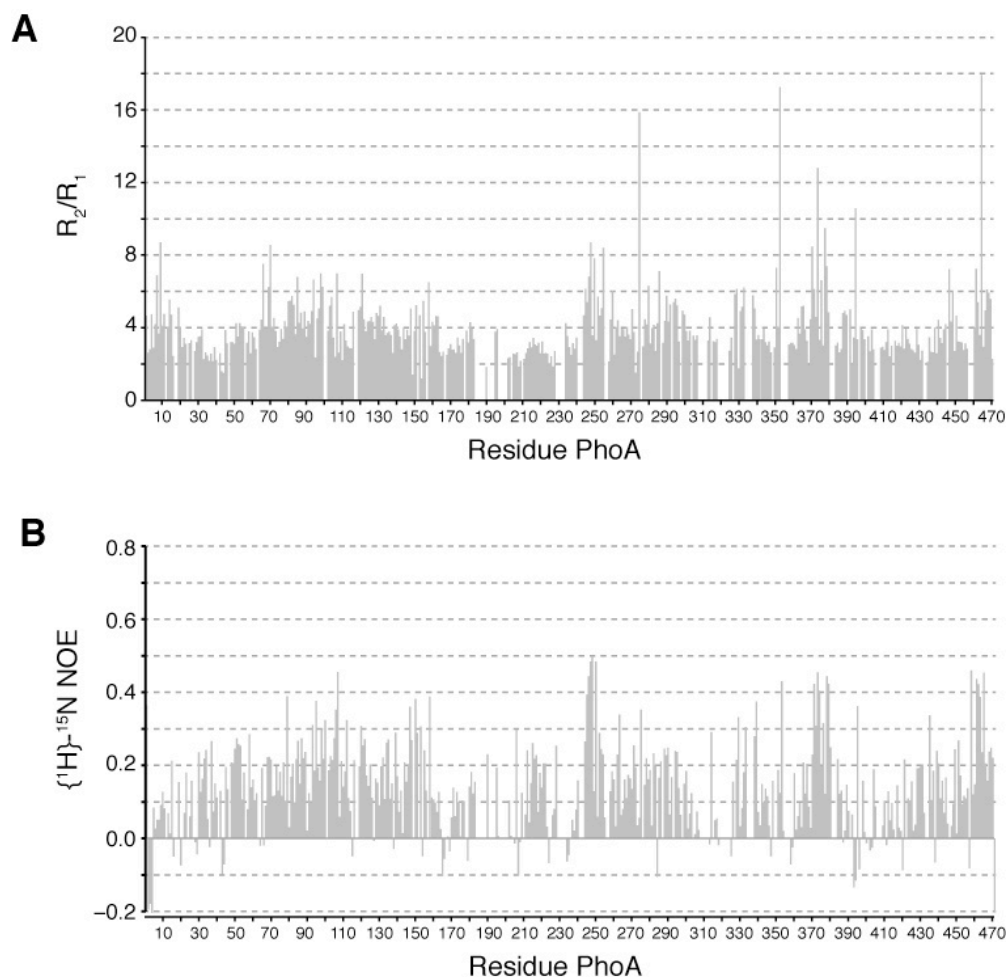


**Fig. S6. Relaxation analysis of unfolded PhoA.** (A)  $^{15}\text{N}$   $R_2/R_1$  values of unfolded PhoA plotted as a function of the amino acid sequence.  $R_2$  and  $R_1$  are the transverse and longitudinal relaxation rates, respectively. Lower values indicate flexibility whereas higher values indicate rigidity (or the presence of conformational exchange). The low  $R_2/R_1$  values throughout the PhoA sequence suggests that the protein indeed is in a disordered state. Certain regions exhibit higher values suggesting the presence of transiently formed secondary structure. (B) Steady-state  $\{^1\text{H}\}$ - $^{15}\text{N}$  values of unfolded PhoA plotted as a function of the amino acid sequence. Values higher than  $\sim 0.7$  are typically found in regions with secondary structure whereas negative or close to zero are found in completely disordered regions. Values of 0.3-0.4 indicate the presence of transiently formed local secondary structure.

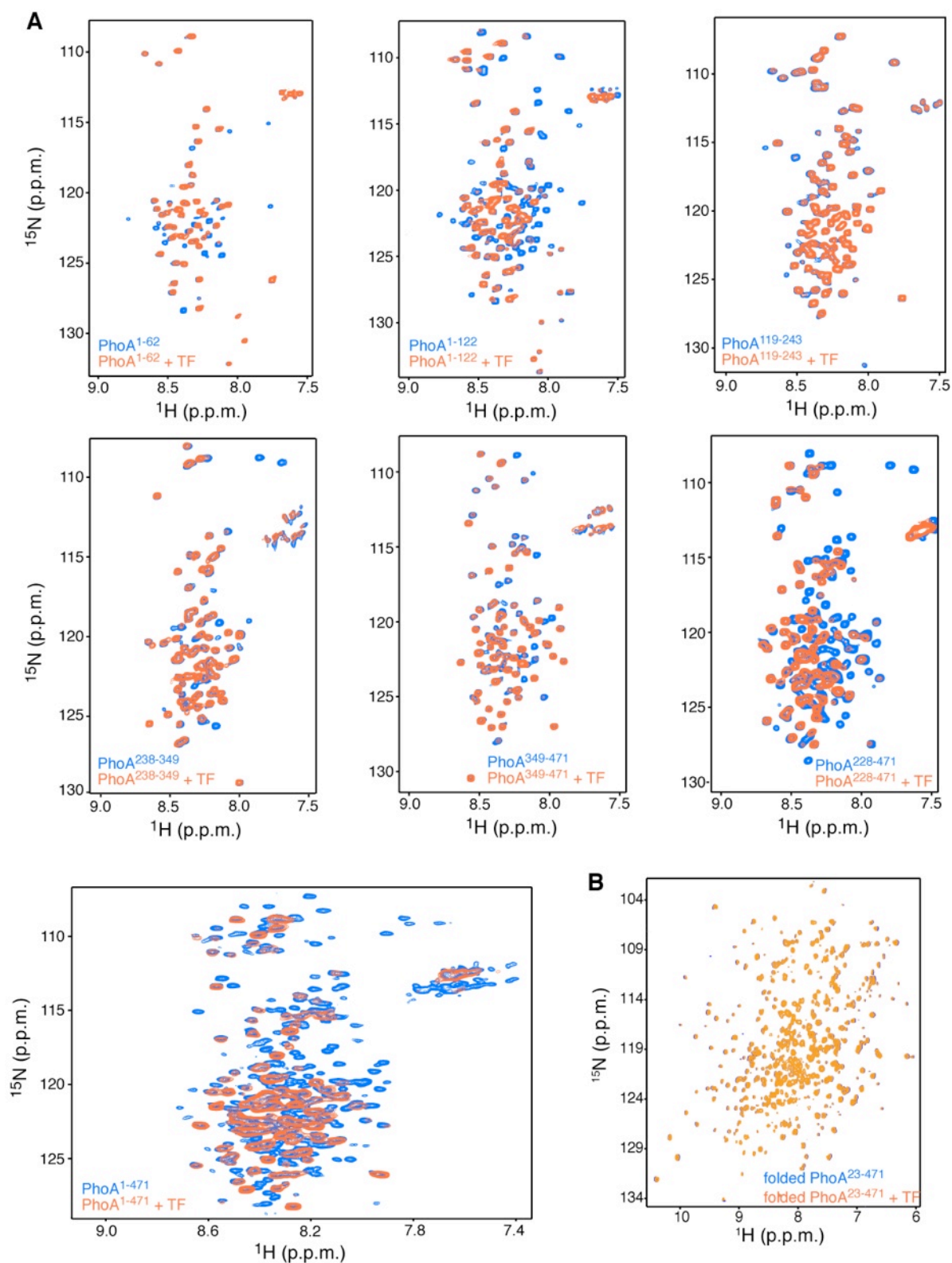


**Fig. S7. Identification of the TF-binding sites in PhoA by NMR. (A)** <sup>15</sup>N labeled full-length PhoA as well as a number of PhoA fragments were titrated with unlabeled TF. Due to the labeling scheme and the size of TF, the intensity of the PhoA residues that are bound by TF decreases dramatically or disappears. The <sup>1</sup>H-<sup>15</sup>N HSQC spectra of PhoA select fragments and the full-length PhoA are shown in the absence (blue) and presence (orange) of TF. The fragments cover the entire sequence of PhoA and the regions identified to interact with TF in the various PhoA fragments are essentially identical to the full-length PhoA. **(B)** Oxidized, folded PhoA (mature form) does not interact with TF.



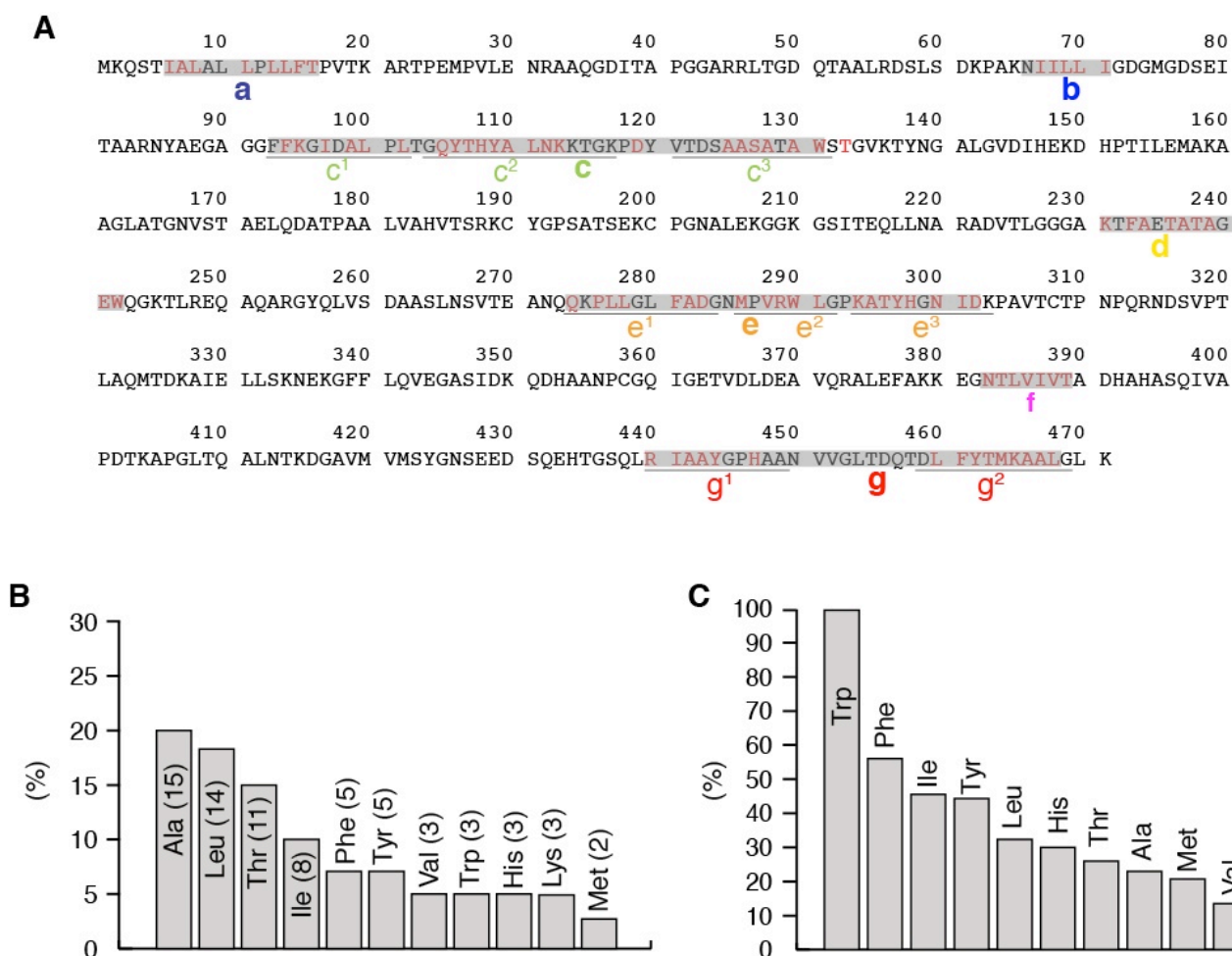


**Fig. S8. Amino acid composition of TF-binding sites in PhoA.** (A) Primary sequence of PhoA with the TF-binding sites (a-g) highlighted. The PhoA residues that form direct contacts with TF are colored red (see Fig. 4). The color code of the sites and subsites are as in Fig. 2C and 3A. (B) Percentage values of the PhoA amino acids that directly interact with TF. The number in brackets correspond to the actual number of amino acids. (C) Percentage values of PhoA amino acids that interact with TF normalized against the total number of each one of the amino acids in the PhoA sequence. For example, all of the three Trp residues in PhoA interact with TF (that is, 100%).

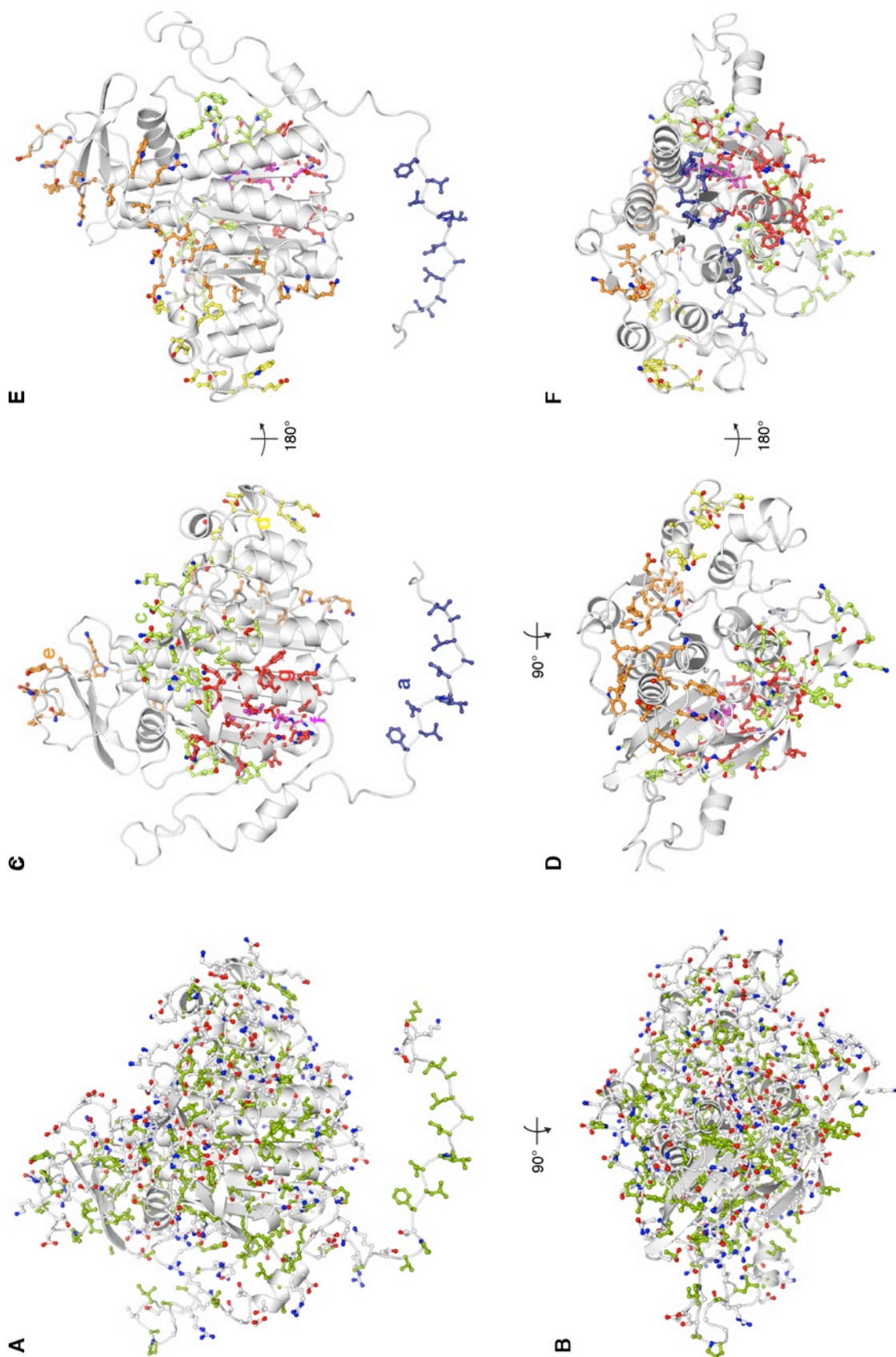


**Fig. S9. Distribution of the TF-binding sites in PhoA mapped on its folded structure.** (A to D) Distribution of nonpolar residues (in green) in the folded structure of PhoA. (C to F) The residues from the seven distinct regions in PhoA (a-g) that interact with TF are shown in sticks.

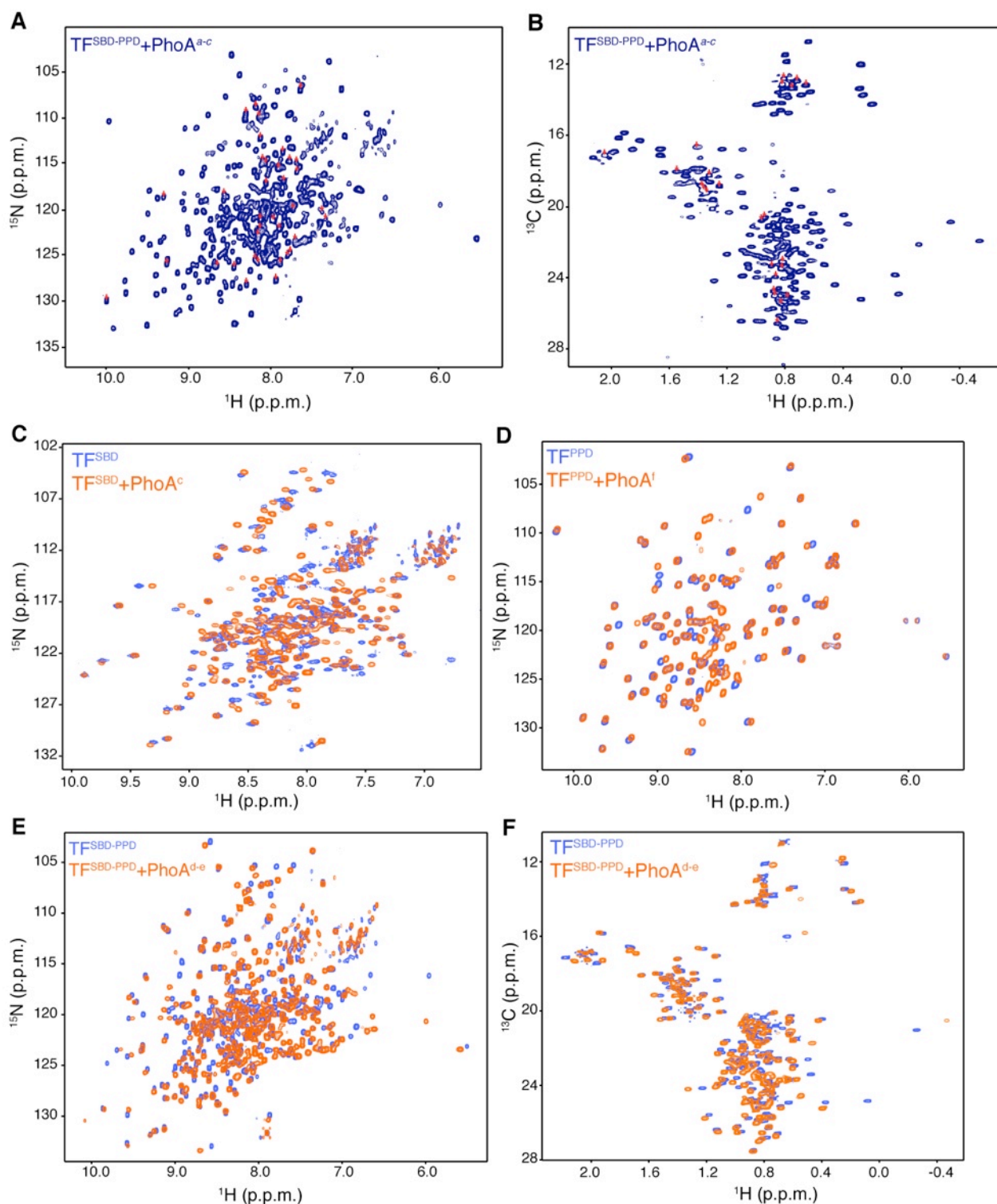


**Fig. S10. NMR spectra of TF in complex with PhoA.** (A,B)  $^1\text{H}$ - $^{15}\text{N}$  HSQC and  $^1\text{H}$ - $^{13}\text{C}$  methyl HMQC spectra of  $[\text{U-}^2\text{H}, ^{15}\text{N}; \text{Ala-}^{13}\text{CH}_3; \text{Met-}^{13}\text{CH}_3; \text{Ile-}\delta 1\text{-}^{13}\text{CH}_3; \text{Leu, Val-}^{13}\text{CH}_3/^{13}\text{CH}_3]$ -labeled  $\text{TF}^{\text{SBD-PPD}}$  in complex with  $\text{PhoA}^{\text{a-c}}$ . The arrows indicate the resonances of PhoA that interact with TF and thus exhibit markedly enhanced resonance dispersion. (C)  $^1\text{H}$ - $^{15}\text{N}$  HSQC spectra of  $[\text{U-}^2\text{H}, ^{15}\text{N}]$ -labeled  $\text{TF}^{\text{SBD}}$  in the free state (blue) and in complex with  $\text{PhoA}^{\text{c}}$  (orange). (D)  $^1\text{H}$ - $^{15}\text{N}$  HSQC spectra of  $^{15}\text{N}$ -labeled  $\text{TF}^{\text{PPD}}$  in the free state (blue) and in complex with  $\text{PhoA}^{\text{f}}$  (orange). (E)  $^1\text{H}$ - $^{15}\text{N}$  HSQC spectra of  $[\text{U-}^2\text{H}, ^{15}\text{N}]$ -labeled  $\text{TF}^{\text{SBD-PPD}}$  in the free state (blue) and in complex with  $\text{PhoA}^{\text{d-e}}$  (orange). (F)  $^1\text{H}$ - $^{13}\text{C}$  methyl HMQC spectra of  $[\text{U-}^2\text{H}; \text{Ala-}^{13}\text{CH}_3; \text{Met-}^{13}\text{CH}_3; \text{Ile-}\delta 1\text{-}^{13}\text{CH}_3; \text{Leu, Val-}^{13}\text{CH}_3/^{13}\text{CH}_3]$ -labeled  $\text{TF}^{\text{SBD-PPD}}$  in the free state (blue) and in complex with  $\text{PhoA}^{\text{d-e}}$  (orange). In all cases both TF and PhoA are similarly labeled.

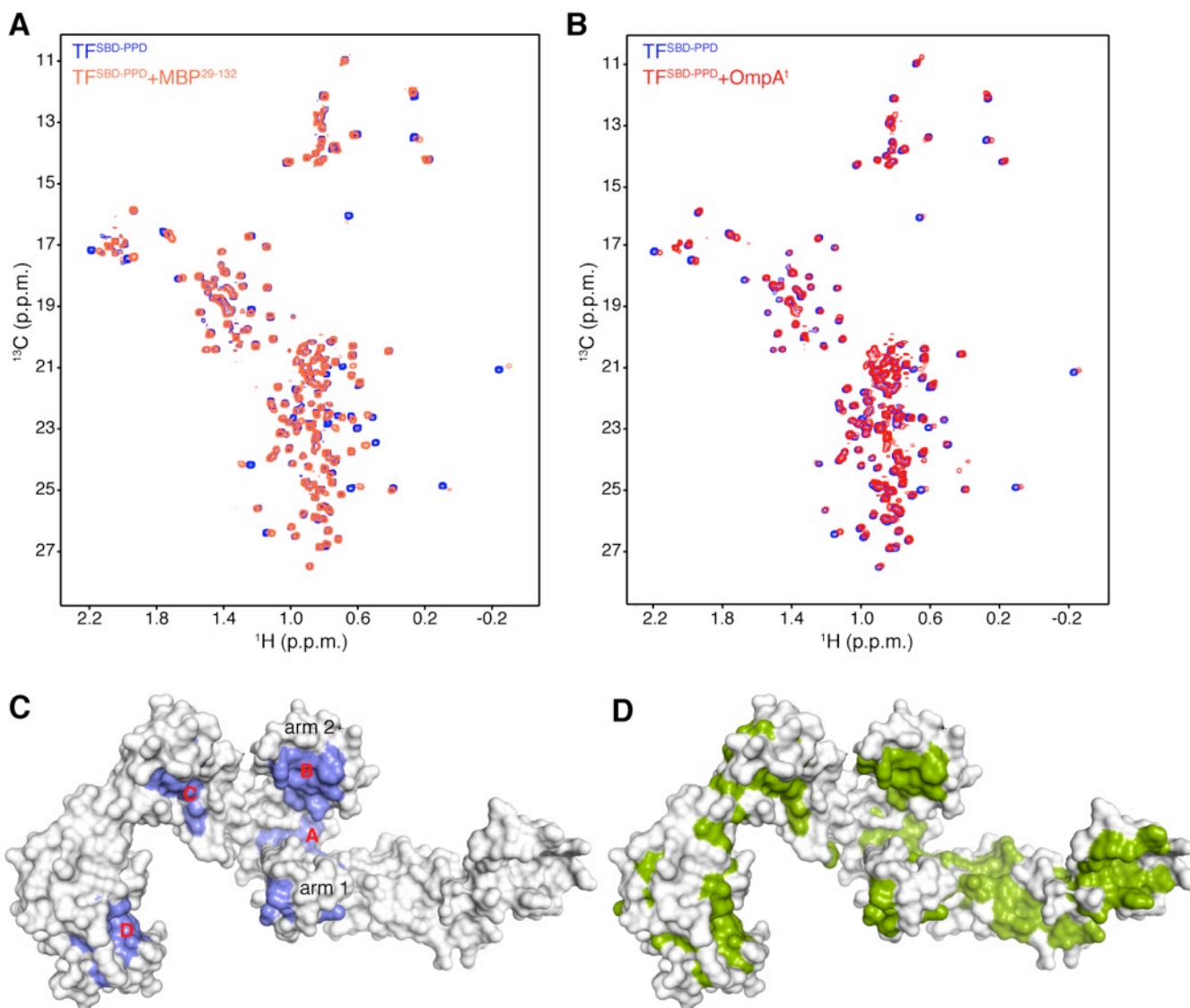


**Fig. S11. Interaction of the TF chaperone module (TF<sup>SBD-PPD</sup>) with unfolded fragments of the maltose binding protein (MBP) and the transmembrane region of OmpA.** (A) <sup>1</sup>H-<sup>13</sup>C HMQC spectra of [U-<sup>2</sup>H,<sup>15</sup>N; Ala-<sup>13</sup>CH<sub>3</sub>; Met-<sup>13</sup>CH<sub>3</sub>; Ile- $\delta$ 1-<sup>13</sup>CH<sub>3</sub>; Leu,Val-<sup>13</sup>CH<sub>3</sub>/<sup>13</sup>CH<sub>3</sub>]-labeled TF<sup>SBD-PPD</sup> in complex with a fragment of unlabeled MBP consisting of residues 29-132, which, based on its hydrophobicity (see fig. S26), is predicted to have several TF-binding sites. (B) <sup>1</sup>H-<sup>13</sup>C HMQC spectra of [U-<sup>2</sup>H,<sup>15</sup>N; Ala-<sup>13</sup>CH<sub>3</sub>; Met-<sup>13</sup>CH<sub>3</sub>; Ile- $\delta$ 1-<sup>13</sup>CH<sub>3</sub>; Leu,Val-<sup>13</sup>CH<sub>3</sub>/<sup>13</sup>CH<sub>3</sub>]-labeled TF<sup>SBD-PPD</sup> in complex with the transmembrane region of OmpA (OmpA<sup>t</sup>, residues 1-190). (C) The TF residues identified by NMR (both from backbone and side chain chemical shifts) to interact with MBP<sup>29-132</sup> and OmpA<sup>t</sup> are colored blue. All four binding sites (A-D) that interact with PhoA also interact with MBP and OmpA. In addition, a hydrophobic region located in arm 1 interacts with MBP and OmpA. As with the other substrate-binding sites, this region is hydrophobic, as can be seen in panel D, which shows the hydrophobic residues in TF (colored green).



**Fig. S12. Sequence conservation of TF.** Sequence logo of TF created from a collection of aligned sequences of TF. 60 unique sequences of bacterial TF were used and the sequence of *E. coli* TF is shown. The filled circles denote the most important residues for interacting with PhoA (orange, site A; red, site B; green, site C; blue, site D). Almost all of the interacting residues are very well conserved, with the hydrophobic nature of the residue being absolutely conserved. The grey circles denote the ribosome-interacting residues (G43-F-R-x-G-x-x-P).

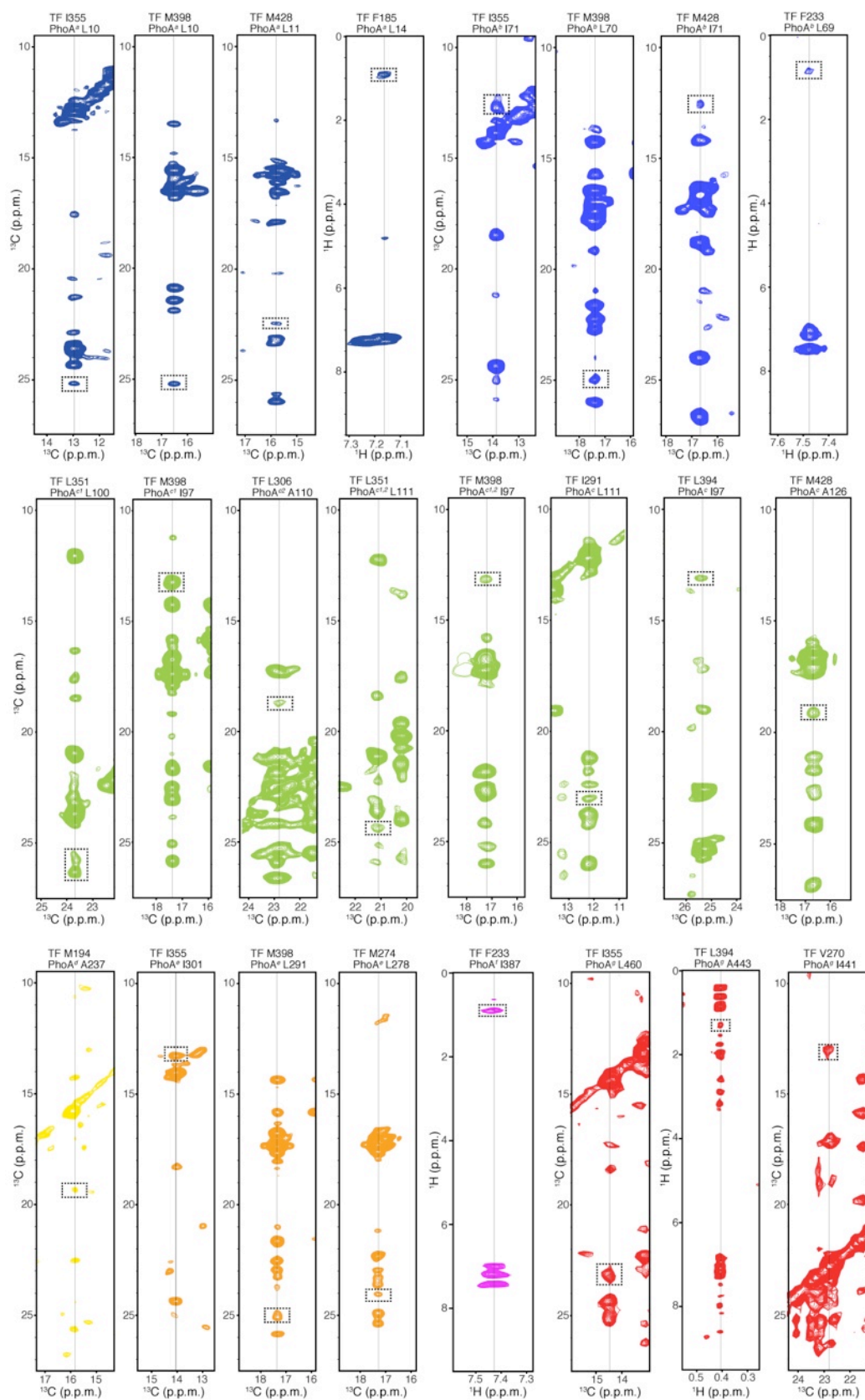


**Fig. S13. Inter-molecular NOEs between TF and PhoA.** The full strips are shown from  $^{13}\text{C}$ -edited NOESY-HSQC and HMQC-NOESY-HMQC NMR experiments corresponding to the inter-NOEs shown in Fig. 3 and fig. S17. The NOE cross-peaks shown in Fig. 3 are designated here by a dashed-line rectangle. The color code of the peaks corresponds to the one used in Fig. 3 and fig. S17.

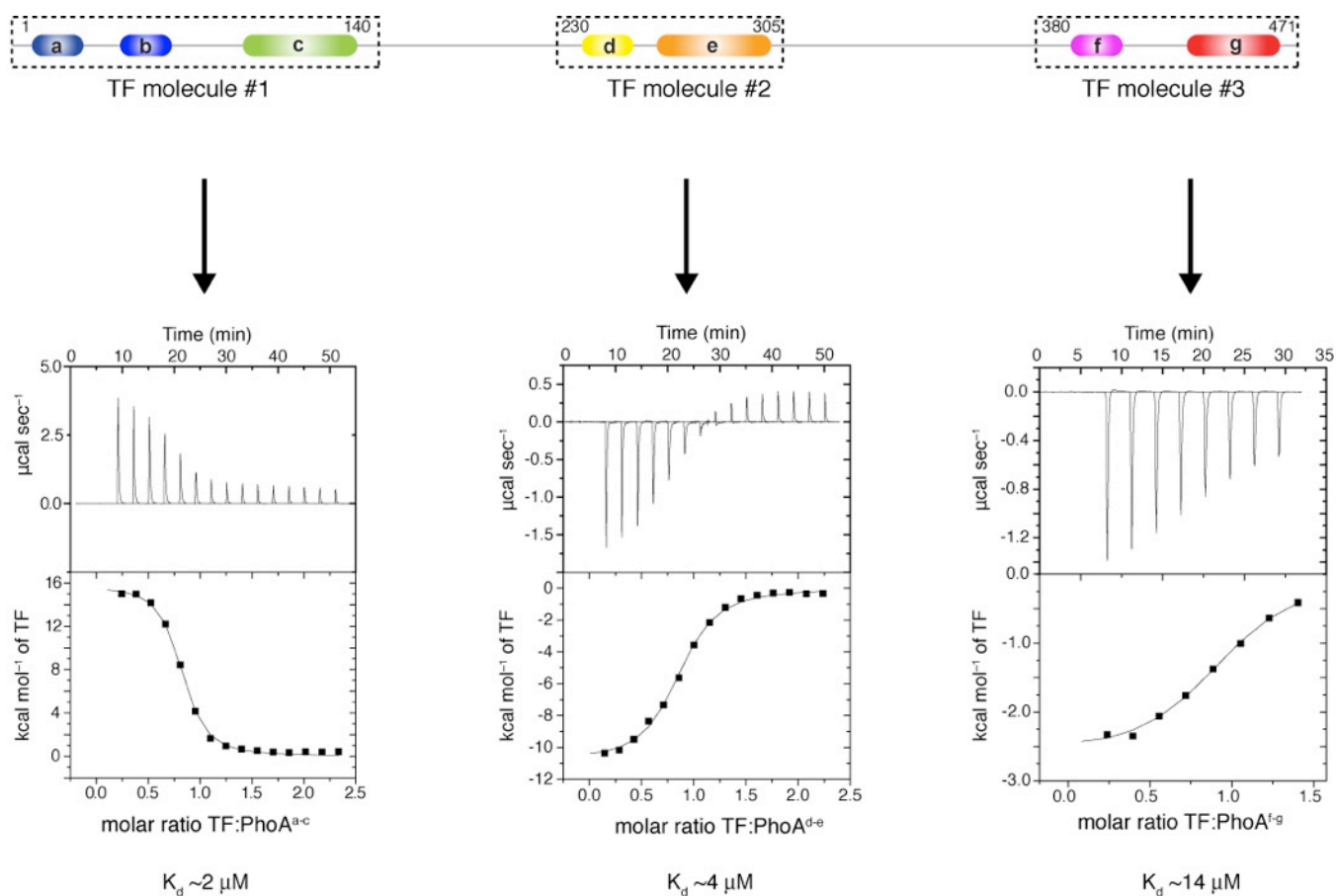


**Fig. S14. Thermodynamic characterization of the interaction between TF and PhoA.** ITC traces of the titration of TF<sup>SBD-PPD</sup> to the three PhoA fragments (PhoA<sup>a-c</sup>, PhoA<sup>d-e</sup>, and PhoA<sup>f-g</sup>). In order to measure pure binding, without contribution from the binding-induced monomerization of TF, the TF<sup>SBD-PPD</sup> fragment was used instead of full-length TF. TF<sup>SBD-PPD</sup> encompasses all of the PhoA binding sites. Although all three complexes are mediated almost exclusively by hydrophobic contacts, the thermodynamic basis of the binding appears to be different for the different complexes. For example, formation of TF<sup>SBD-PPD</sup>-PhoA<sup>a-c</sup> is entropy driven whereas formation of TF<sup>SBD-PPD</sup>-PhoA<sup>d-e</sup> is enthalpy driven. The different thermodynamic signatures likely reflect differences in the degree of immobilization of the flexible linkers tethering the binding sites in PhoA. Stoichiometry for all complexes is TF<sup>SBD-PPD</sup>:PhoA 1:1. The experiments shown here were recorded at 10 °C.

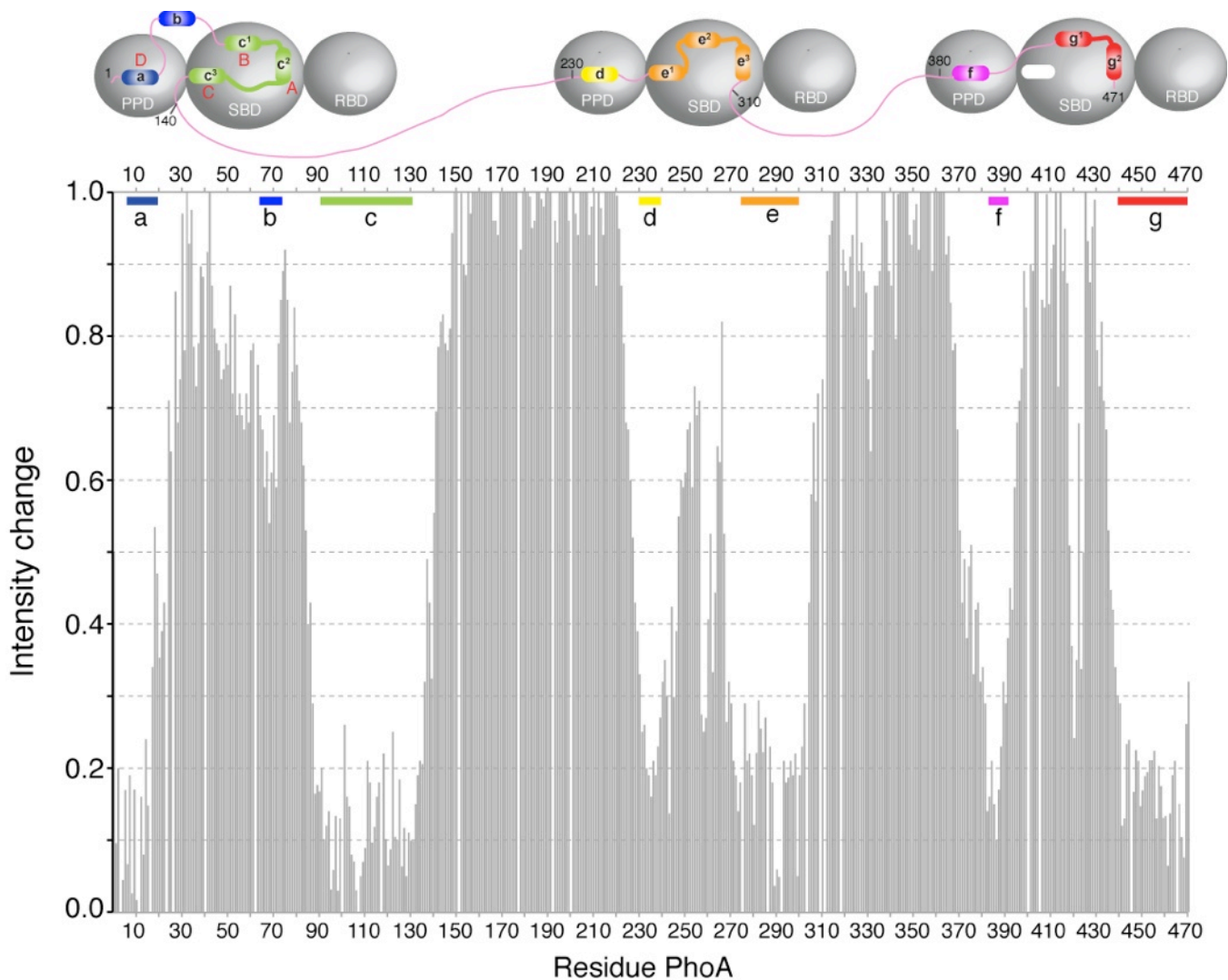


**Fig. S15. NMR resonance intensity analysis of the TF–PhoA complex.** Plot of resonance intensity changes of PhoA residues as a result of complex formation with TF. Because of the labeling scheme used, PhoA residues that are bound by TF have negligible intensity remaining in the complex, whereas the intensity of residues that are not bound by TF, and are thus motionally not restricted, is not significantly affected. Because of the large size of the TF–PhoA complex, transient interaction of PhoA regions with TF can also result in intensity decrease. The PhoA regions consisting of residues 150–220 and 320–370 do not interact with TF and function as flexible linkers that tether the three PhoA-bound TF molecules.



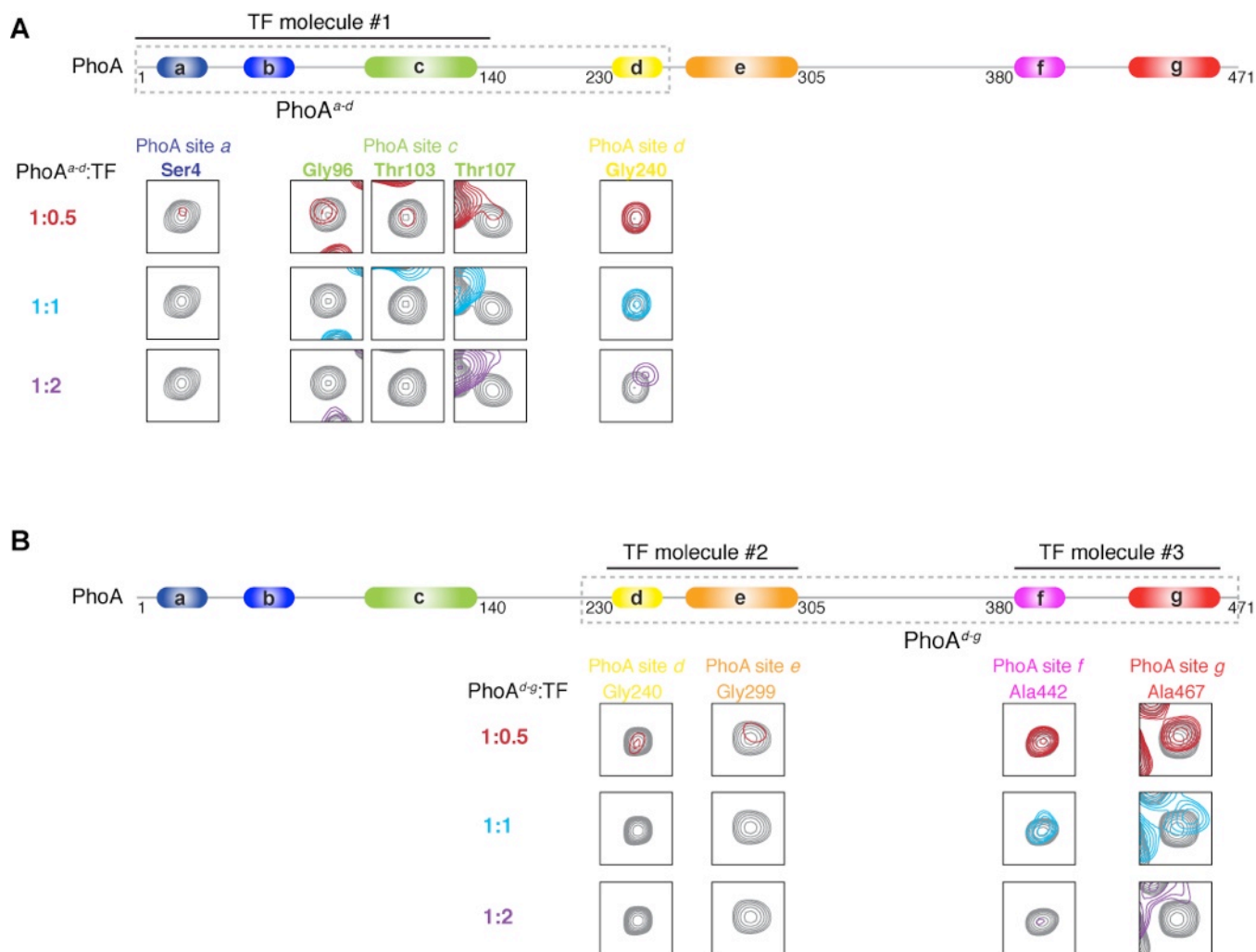


**Fig. S16. Synergistic binding and selectivity of PhoA sites for TF.** (A) As we explain in detail in Fig. 3, one TF molecule can accommodate sites *a* and *c* (residues 1-140). When a longer PhoA fragment that extends to include PhoA site *d* (PhoA<sup>a-d</sup>) is used, then at a stoichiometric ratio of 1:1 (PhoA<sup>a-d</sup>:TF) site *d* is not bound by TF. This is clearly demonstrated by the fact that the chemical shift of Gly240 (located in PhoA site *d*) is not affected at all. When excess of TF is added (PhoA<sup>a-d</sup>:TF 1:2) then site *d* is bound by TF. (B) Direct evidence for synergistic binding among PhoA sites to TF is provided in this experiment. A PhoA fragment consisting of sites *d* through *g* was used (PhoA<sup>d-g</sup>). Isolated sites *d* and *f* bind exclusively to TF PPD (fig. S17B,E) and with very similar affinities (~240  $\mu$ M). One TF molecule binds to PhoA sites *d* and *e*, and another TF molecule binds to PhoA sites *f* and *g* (Fig. 4A and fig. S17). At substoichiometric PhoA<sup>d-g</sup>:TF ratio, only PhoA site *d*, but not PhoA site *f*, is bound to TF because of the higher affinity of the PhoA<sup>d-e</sup> fragment, compared to PhoA<sup>f-g</sup>, for TF (fig. S14). At a PhoA<sup>d-g</sup>:TF ratio of 1:1, only a small fraction of sites *f* and *g* are bound, as dictated by the Boltzmann distribution. Representative peaks from <sup>1</sup>H-<sup>15</sup>N HSQC spectra of labeled TF (TF<sup>SBD-PPD</sup>) free (grey) and in complex (red, blue and purple for PhoA:TF ratio 1:0.5, 1:1 and 1:2, respectively) with the corresponding PhoA site are shown. We should note that due to the labeling scheme used for this experiment, and the size of TF, the intensity of the PhoA residues that are bound by TF decreases dramatically or disappears when binding is strong.

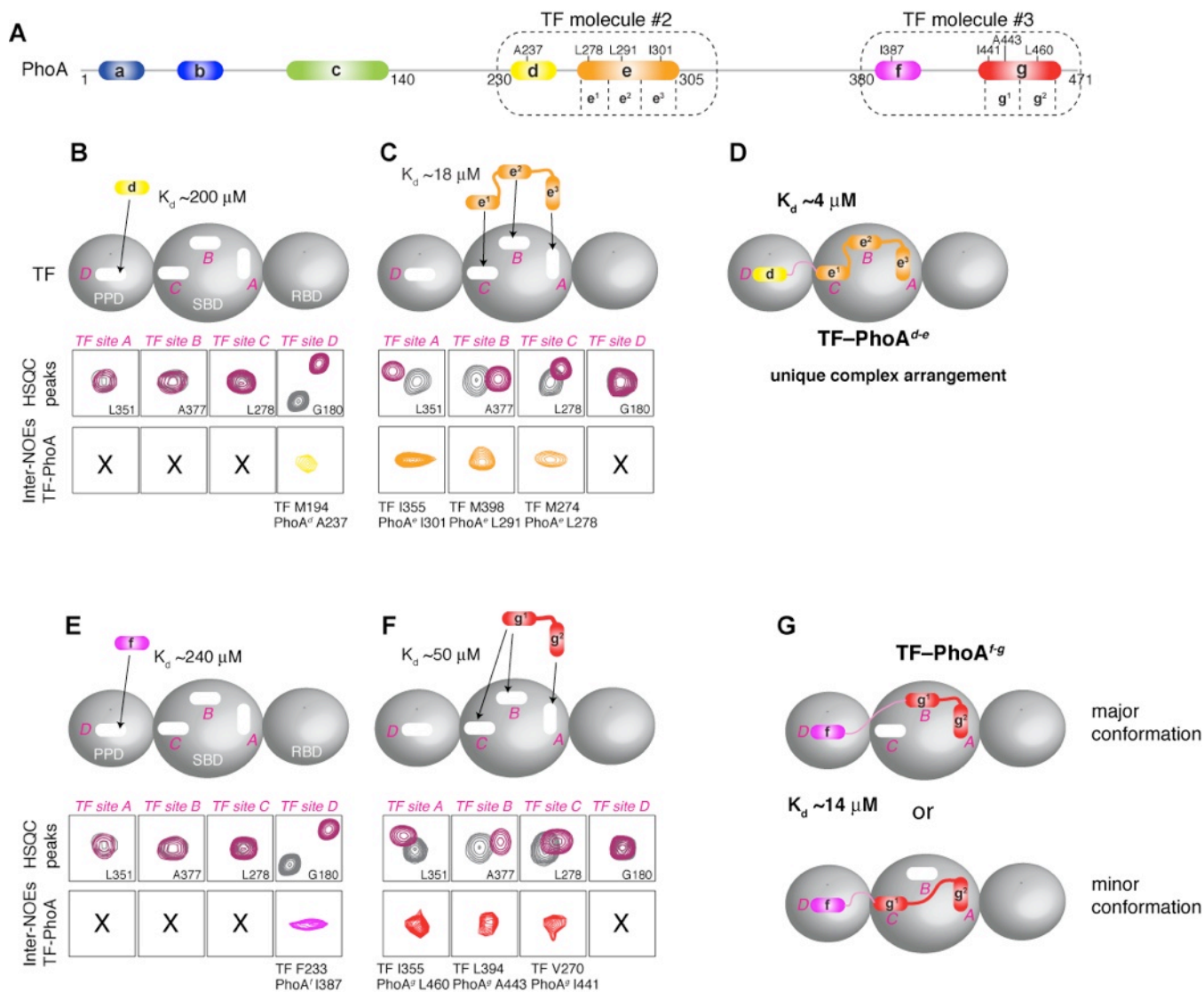


**Fig. S17. Binding of the second and third TF molecules to PhoA sites *d* through *g*.** This figure is an extension of Fig. 3 where the detailed characterization of the binding of PhoA sites *a*, *b* and *c* (subsites *c*<sup>1</sup>, *c*<sup>2</sup>, and *c*<sup>3</sup>) to TF is described. **(A)** TF-binding sites in PhoA colored as in Fig. 3A. PhoA sites *d* and *g* are engaged by one TF molecule (#2) and sites *f* and *g* by an additional TF molecule (#3). PhoA residues whose inter-molecular NOEs to TF residues are depicted on panels B, C, E and F are indicated. In this figure we provide evidence about the selective binding of PhoA site *d* (in **B**), site *e* (in **C**), site *f* (in **E**) and site *g* (in **F**). A unique complex arrangement is observed for the TF-PhoA<sup>*d-e*</sup> complex (in **D**), whereas two binding arrangements are observed for TF-PhoA<sup>*f-g*</sup> complex: in the latter case one of them is more populated (major) than the alternative one (minor). The structure of the major conformation was determined. The full strips of the inter-molecular TF-PhoA NOEs are shown in fig. S13.

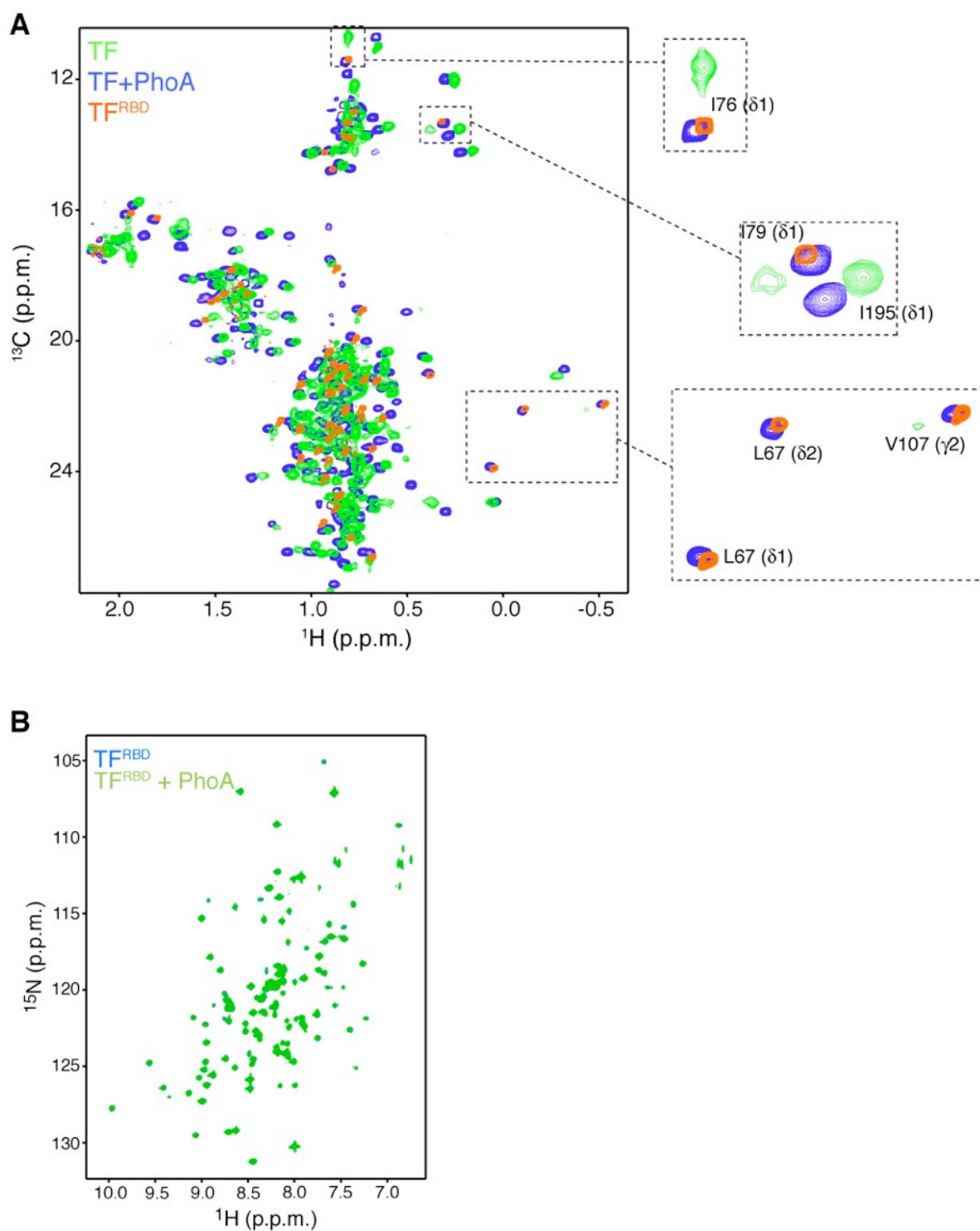


**Fig. S18. PhoA binding monomerizes TF.** (A)  $^1\text{H}$ - $^{13}\text{C}$  HSQC spectra of TF (green), in complex with unlabeled PhoA (blue), and isolated RBD (orange). TF and  $\text{TF}^{\text{RBD}}$  are [ $\text{U}\text{-}^2\text{H}$ ,  $^{15}\text{N}$ ; Ala- $^{13}\text{CH}_3$ ; Met- $^{13}\text{CH}_3$ ; Ile- $\delta 1$ - $^{13}\text{CH}_3$ ; Leu, Val- $^{13}\text{CH}_3$ / $^{13}\text{CH}_3$ ] labeled. Analysis of the spectra shows that several resonances in free TF, which is dimeric (fig. S1C), are broadened beyond detection, presumably because of slow motions at the dimeric interface (fig. S19). NMR analysis demonstrates that TF dimerization is mediated by all three domains (RBD, SBD, and PPD) but RBD resonances in TF are particularly affected (fig. S19). Indeed, monomerization of TF upon PhoA binding (fig. S1C-E) results in the appearance of all of the expected resonances (see for example residues L67, I76, I79 and V107). Furthermore, chemical shift comparison between isolated RBD (orange) and TF in complex with PhoA (blue) suggests that RBD does not bind to PhoA. (B) This observation is further corroborated by NMR titration data of  $^{15}\text{N}$  labeled RBD with PhoA (green). The  $^1\text{H}$ - $^{15}\text{N}$  HSQC spectra show no perturbation.

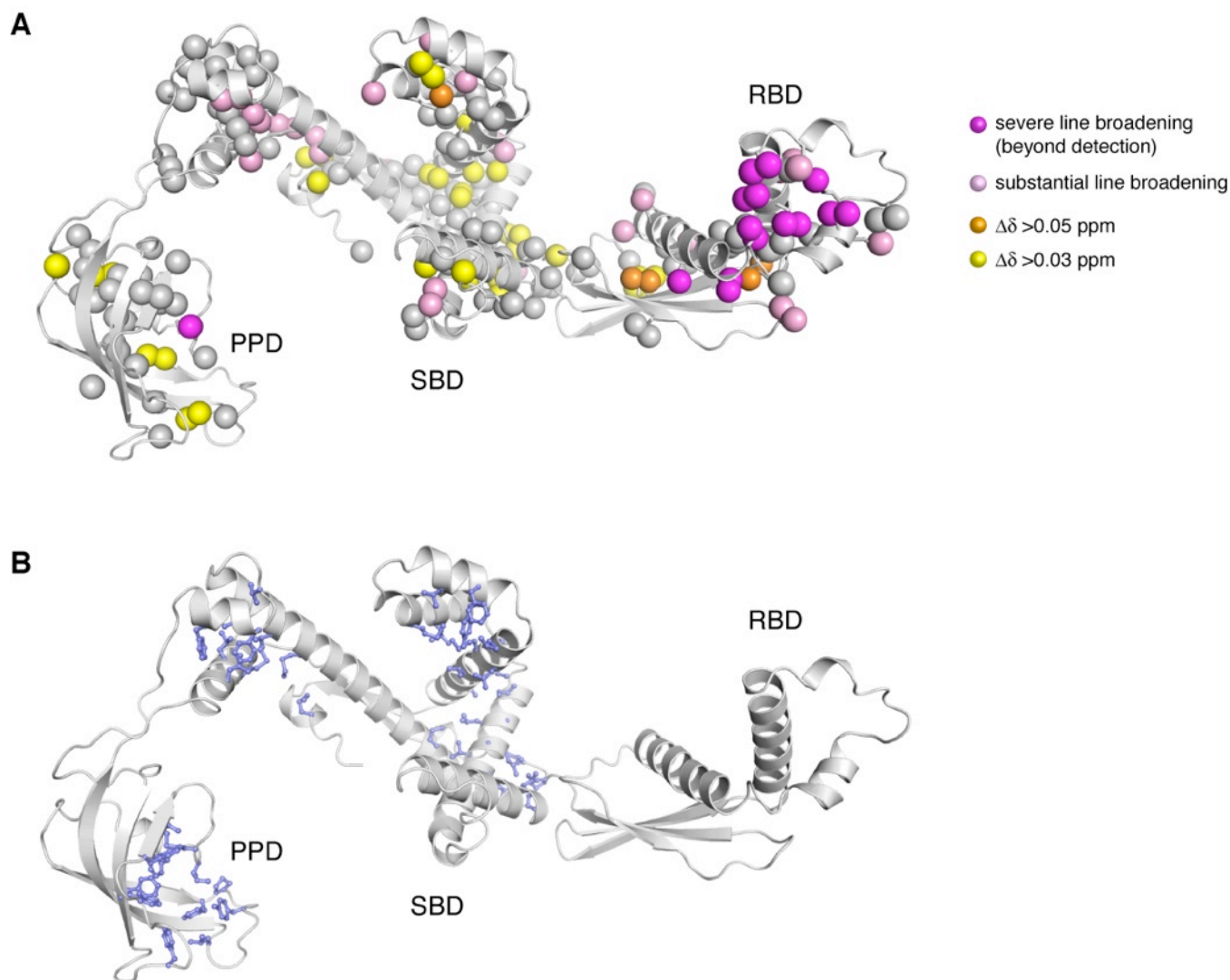


**Fig. S19. Changes in chemical shift and slow dynamics between monomeric and dimeric TF.** (A) Chemical shift changes ( $\Delta\delta$ ) of methyl resonances between monomeric and dimeric TF. The chemical shifts of monomeric TF were obtained in complex with PhoA or using TF<sup>SBD-PPD</sup>. Residues whose resonances are significantly broadened are also indicated. Line broadening (see fig. S18A) is a result of the presence of slow (micro-to-millisecond) dynamics. Line broadening is severe for several residues in TF dimer, whereas TF monomerization suppresses these slow dynamics. Therefore, the residues experiencing such slow motions are very likely located at the dimeric interface. Regions most affected are located in RBD, the tips of the SBD arms and the PPD. These results are in agreement with the dimerization interface seen in the crystal structure of dimeric TF in complex with the S7 protein (27). (B) Residues that make up the four substrate-binding sites in TF are shown in blue. The combined data suggest that some of the substrate-binding regions may be partially occluded in TF dimer, explaining why PhoA binding to TF results in TF monomerization.

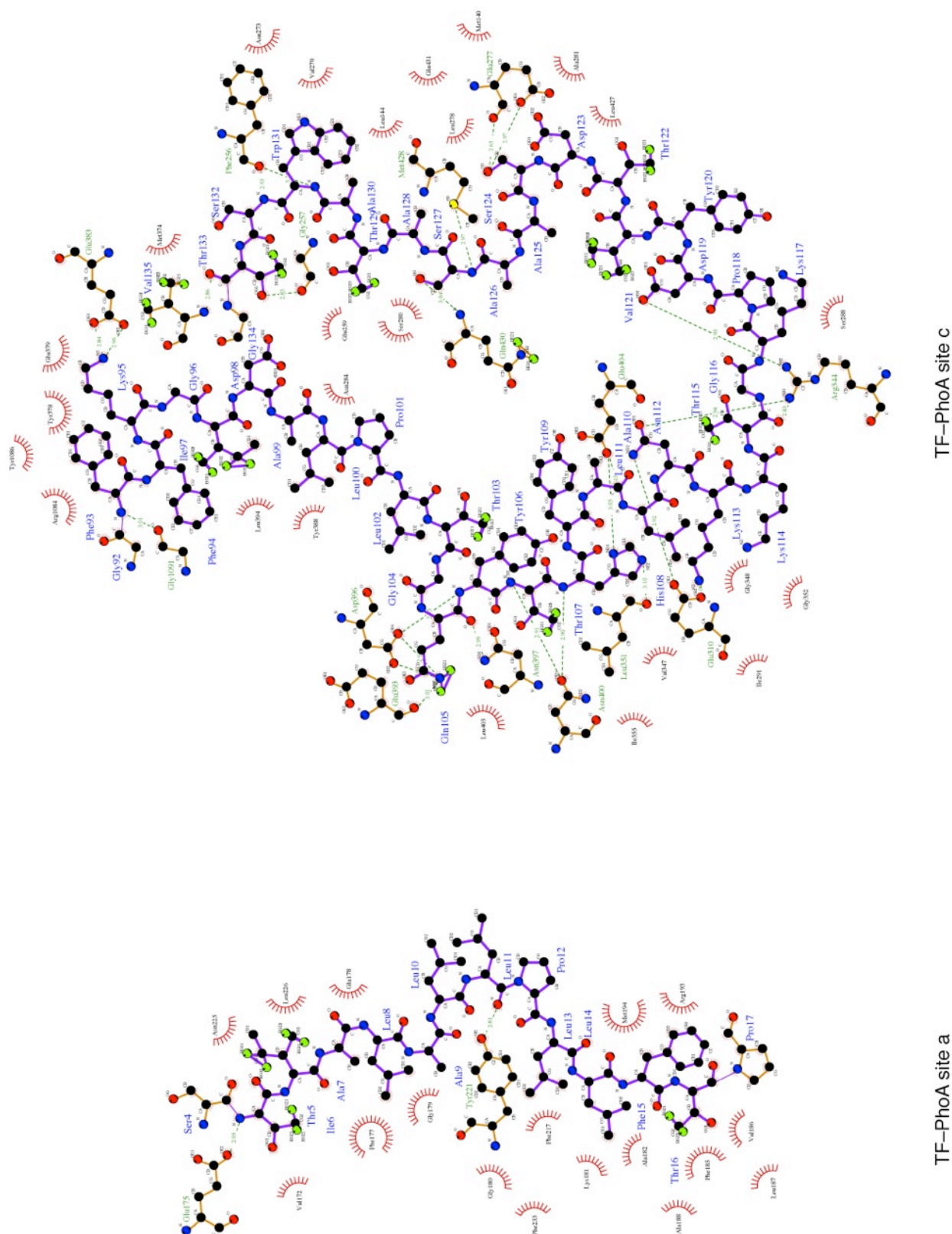


**Fig. S20. TF-PhoA<sup>a-c</sup> contacts.** Inter-molecular contacts between TF and PhoA<sup>a-c</sup> generated by Ligplot (<http://www.ebi.ac.uk/thornton-srv/software/LIGPLOT/>).

**TF molecule #1**

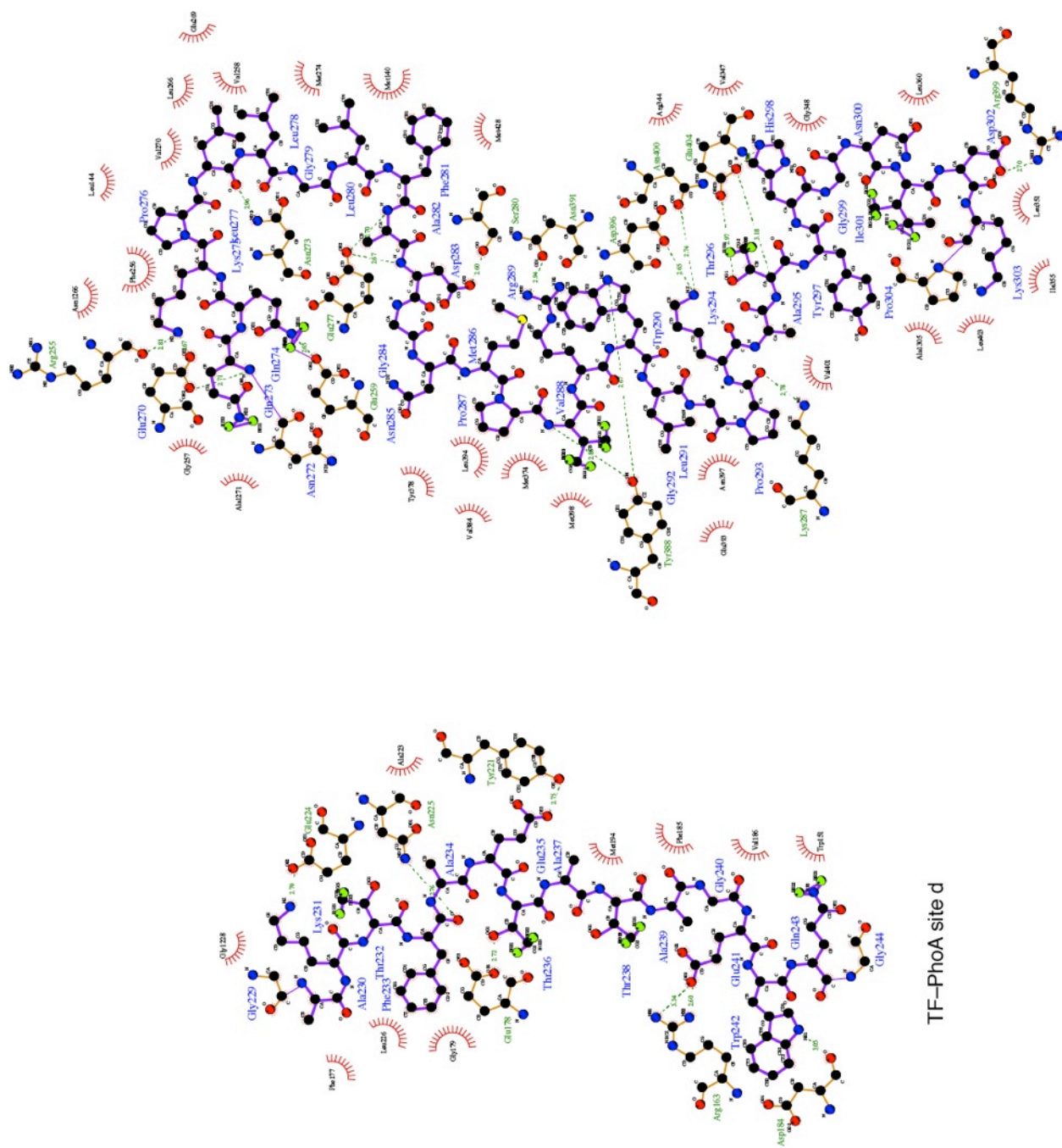
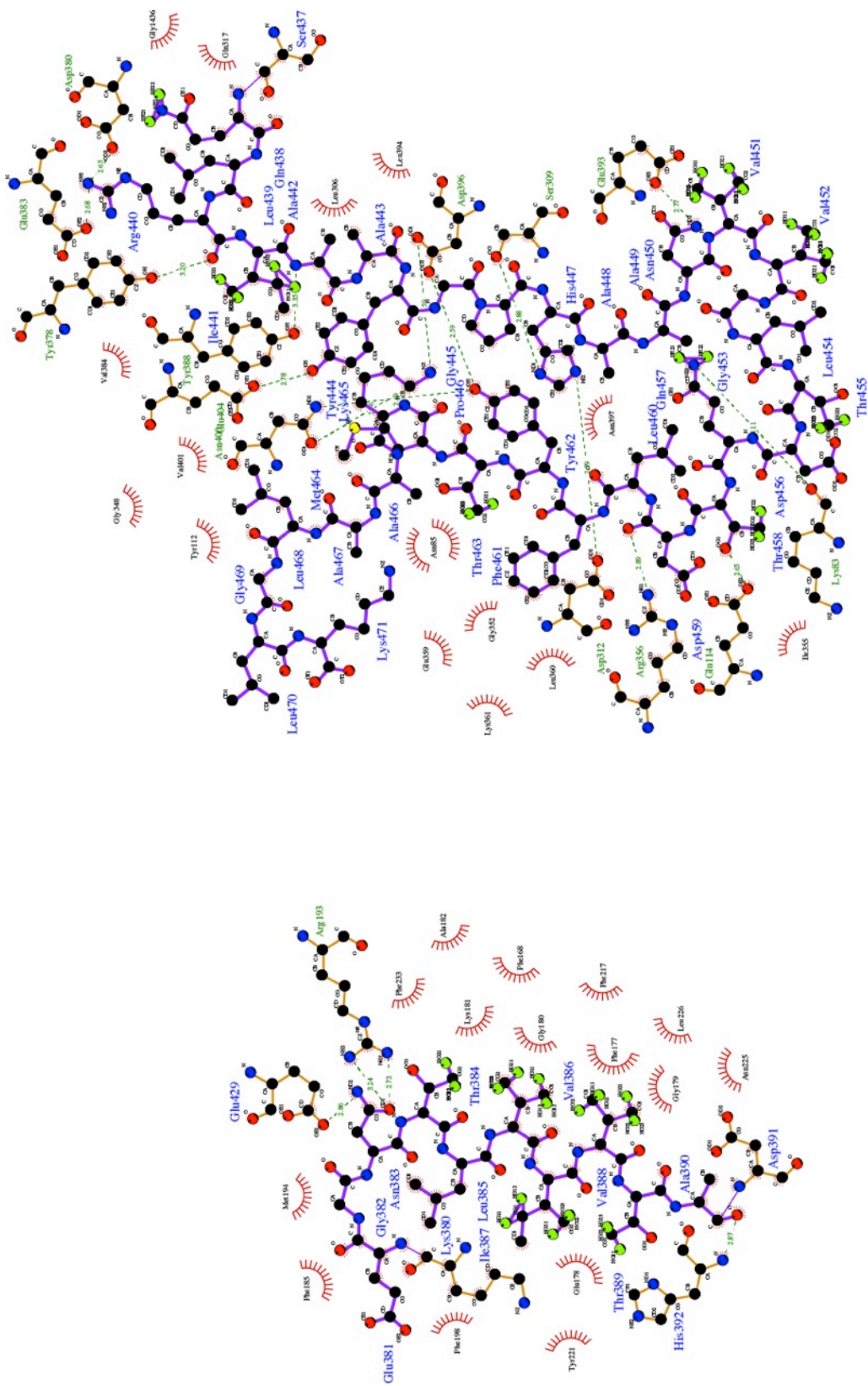


Fig. S21. TF–PhoA<sup>d-e</sup> contacts. Inter-molecular contacts between TF and PhoA<sup>d-e</sup> generated by Ligplot.

TF–PhoA site e

TF molecule #2

TF–PhoA site d

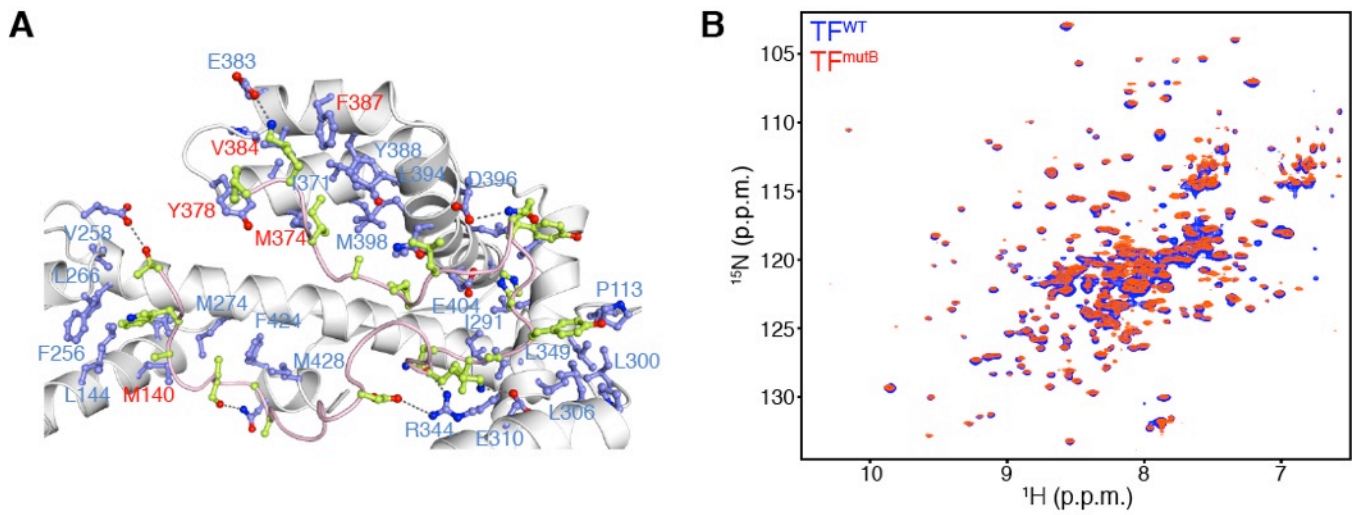


TF-PhoA site g

TF-PhoA site f

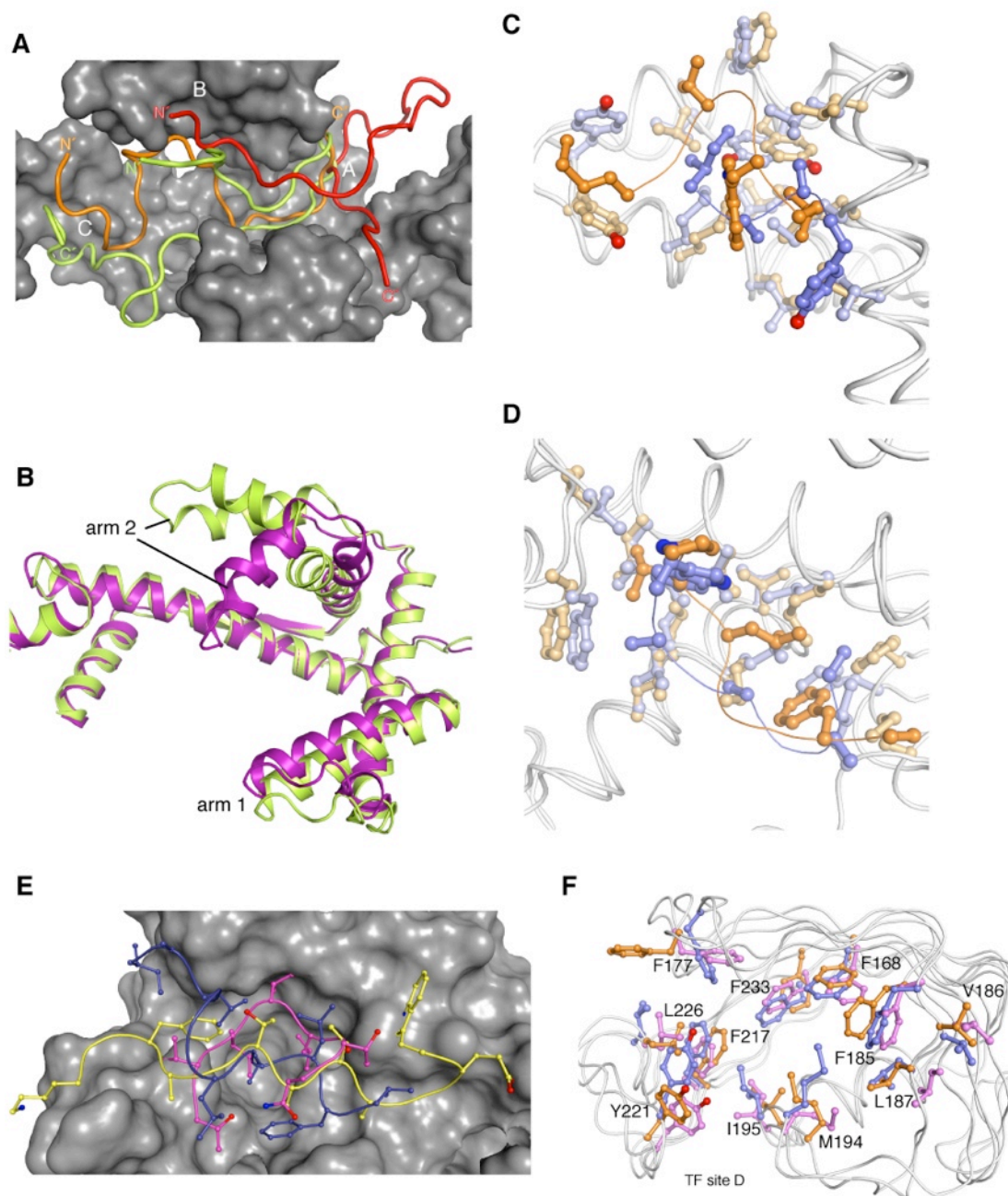
### TF molecule #3

Fig. S22. TF-PhoA<sup>fg</sup> contacts. Inter-molecular contacts between TF and PhoA<sup>fg</sup> generated by Ligplot.



**Fig. S23. Mutations in substrate-binding sites of TF.** (A) Location of selected amino-acid substitution sites highlighted in red. Four of them (M374A, Y378A, V384A, F387A) are located in the B site, with the corresponding TF mutant referred to as  $\text{TF}^{\text{mutB}}$ , whereas the M140E substitution is located in the C site and thus the corresponding TF mutant is referred to as  $\text{TF}^{\text{mutC}}$  (see materials and methods for more information about the various mutants). (B)  $^1\text{H}$ - $^{15}\text{N}$  HSQC spectra of wild type TF ( $\text{TF}^{\text{WT}}$ , blue) and  $\text{TF}^{\text{mutB}}$  (red). The spectra clearly show that  $\text{TF}^{\text{mutB}}$  is well folded. The results of the effect of these mutations on the activity of TF are shown in Fig. 5.





**Fig. S24. Conformational plasticity and heterogeneity in TF-PhoA interactions.** (A) Superposition of the three structures of TF SBD in complex with PhoA sites *c* (green), *e* (orange), and *g* (red). SBD is shown as dark grey solvent-accessible surface whereas PhoA sites are shown in ribbon. (B) Superposition of two TF conformers indicating the dynamic character of arm 2. This flexibility was also seen in the two TF molecules in the crystallographic asymmetric unit (12). (C,D) Superimposed structures of TF site B (in C) and site C (in D) in two of the complexes. Both TF and PhoA are shown. TF side chains are colored light blue and light orange in the two complexes whereas PhoA side chains are colored dark blue and dark orange in the corresponding complexes. The figures demonstrate the different interactions between TF and PhoA in the two complexes. (E) Superimposed structures of the three structures of TF PPD in complex with their PhoA sites (site *a* is in blue), *d* is in yellow, and *f* is in magenta. PPD is shown as dark grey solvent-accessible surface whereas PhoA sites are shown in ribbon. The PhoA residues that interact with PPD are shown as sticks. (F) Side chain rearrangements in the three complexes between TF and PhoA sites *a*, *d*, and *f*. The TF side chains are shown as sticks and are colored blue, orange and magenta in TF-PhoA<sup>*a*</sup>, TF-PhoA<sup>*d*</sup>, and TF-PhoA<sup>*f*</sup>, respectively. PhoA is not shown for clarity.

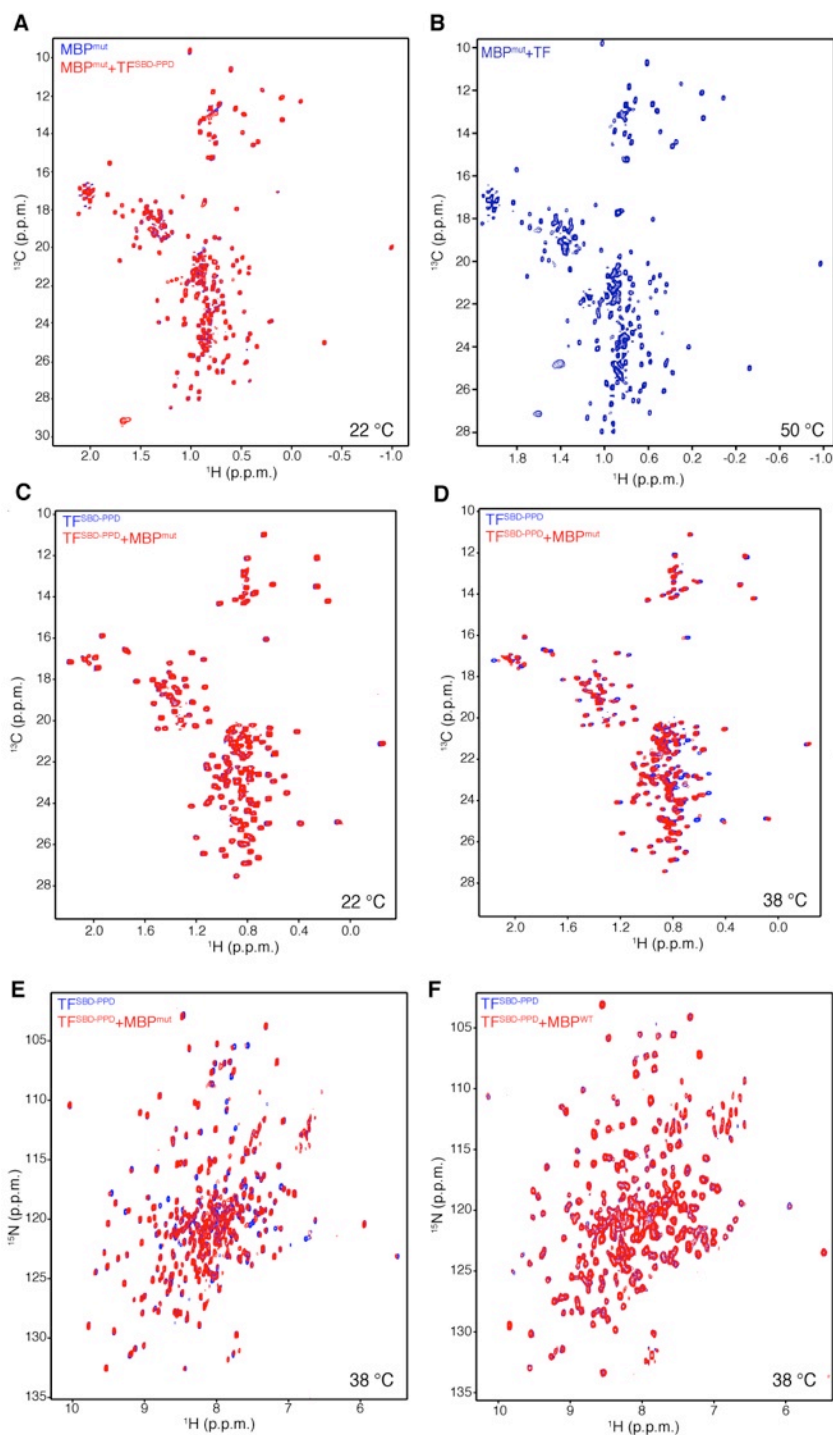


**Fig. S25. TF binds to the unfolded state of MBP<sup>mut</sup>.** (A)  $^1\text{H}$ - $^{13}\text{C}$  HMQC spectra of MBP<sup>mut</sup> free and in complex with TF<sup>SBD-PPD</sup> recorded at 22 °C. The data show no binding. (B)  $^1\text{H}$ - $^{13}\text{C}$  HMQC spectra of MBP<sup>mut</sup> in complex with TF recorded at 50 °C. MBP<sup>mut</sup> suffers heavy precipitation and aggregation at temperatures higher than 30 °C, but in the presence of TF it is stable and folded even at temperatures as high as 50 °C. (C)  $^1\text{H}$ - $^{13}\text{C}$  HMQC of TF<sup>SBD-PPD</sup> free and in complex with MBP<sup>mut</sup>. This experiment is similar to the one shown in panel A but with reverse labeling. No binding was detected at 22 °C between the folded state of MBP<sup>mut</sup> and TF. (D)  $^1\text{H}$ - $^{13}\text{C}$  HMQC of TF<sup>SBD-PPD</sup> free and in complex with MBP<sup>mut</sup> at 38 °C. Because of the elevated temperature, a significant unfolded population of MBP<sup>mut</sup> is present, which binds to TF. (E)  $^1\text{H}$ - $^{15}\text{N}$  HSQC spectra of TF<sup>SBD-PPD</sup> free and in complex with MBP<sup>mut</sup> at 38 °C. (F)  $^1\text{H}$ - $^{15}\text{N}$  HSQC spectra of TF<sup>SBD-PPD</sup> free and in the presence of MBP<sup>WT</sup>. No binding was detected between the two proteins. For the entire series of experiments, the effect of MBP<sup>mut</sup> or MBP<sup>WT</sup> binding to full-length TF or TF<sup>SBD-PPD</sup> are essentially identical and so TF and TF<sup>SBD-PPD</sup> were used interchangeably. Proteins were [U- $^2\text{H}$ ,  $^{15}\text{N}$ ; Ala- $^{13}\text{CH}_3$ ; Met- $^{13}\text{CH}_3$ ; Ile- $\delta 1$ - $^{13}\text{CH}_3$ ; Leu, Val- $^{13}\text{CH}_3$ / $^{13}\text{CH}_3$ ] labeled.

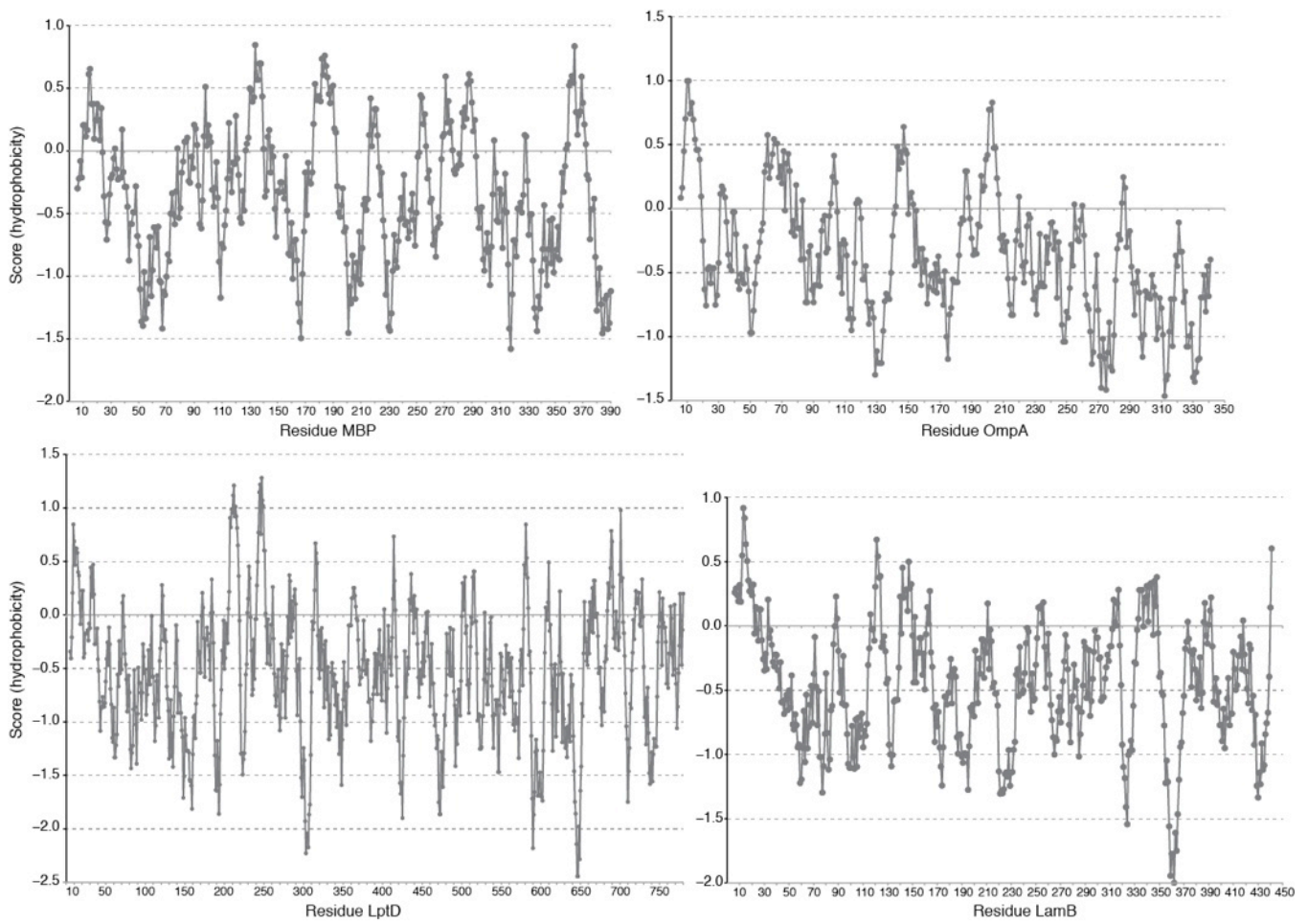


**Fig. S26. Sequence hydrophobicity for *E. coli* proteins previously identified to bind strongly to TF (25).** Plot of the hydrophobicity of MBP, OmpA, LTD and LamB as a function of its primary sequence. A hydrophobicity score (Roseman algorithm, window=9) higher than zero denotes increased hydrophobicity.

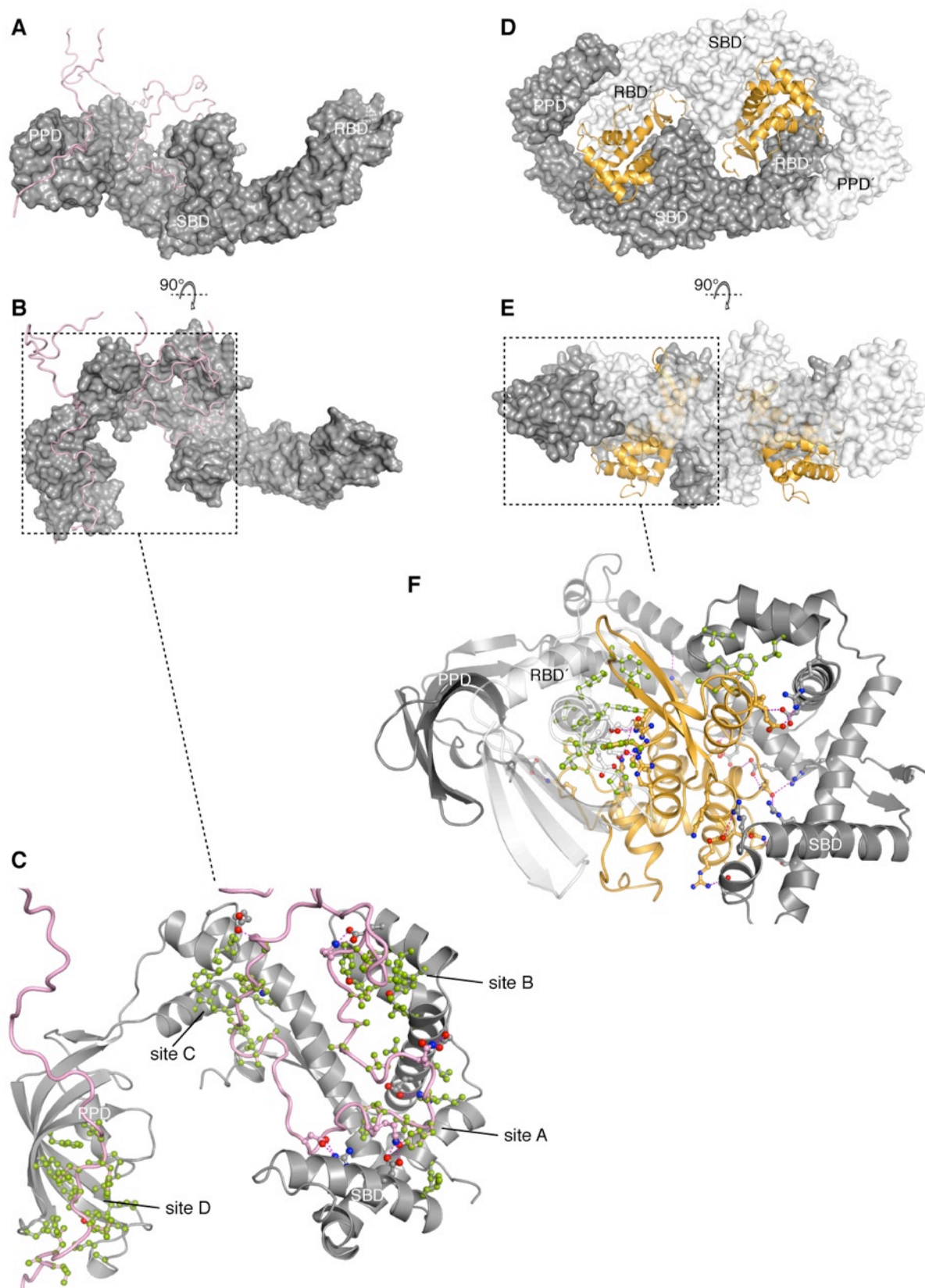


**Fig. S27. Functional versatility of TF.** In addition to the well characterized binding activity of TF for unfolded proteins, it has been recently observed (27) that small proteins can bind in a folded state to a cavity formed in the dimeric TF. **(A to C)** Structural basis for the interaction of TF with unfolded proteins, as determined in this work. TF is shown in a grey solvent-accessible surface and PhoA is shown in a pink ribbon. **(D to F)** Structural basis for the interaction of TF with small folded proteins as determined previously by crystallography (27). TF is dimeric (the two

subunits are shown in grey and semi-transparent white surface) and the folded protein (ribosomal protein S7) in orange. The TF–S7 complex is from *thermotoga maritima*. Views in **A** and **B** (**D** and **E**) are related by a 90° rotation about the x axis. S7 binds in a cavity that is formed by the SBD and PPD of one subunit and the RBD of the other subunit. The majority of the contacts between S7 and TF are polar (H-bonds and salt bridges, denoted with the magenta broken lines), with only few hydrophobic contacts (hydrophobic residues are shown in green, panel **f**). In contrast, in the TF–PhoA complex, the vast majority of the contacts are hydrophobic (panel **c**). TF dimerization appears to be essential for the stabilization of the TF–S7 complex, whereas TF is forced to monomerize in the TF–PhoA complex. Further experiments are required in order to understand whether TF monomerization is substrate-length dependent and how TF can apparently bind both to unfolded as well as folded proteins. It should be noted that several large (over 30 kDa) folded proteins, such as PhoA and MBP, were tested and were found not to interact with TF. Therefore, it seems that TF can bind only to relatively small folded proteins as they will have to fit inside the cavity formed by the two TF subunits.

**Table S1.** Structural and NMR statistics of the three TF-PhoA complexes.

Complex	TF-PhoA <sup>a-c</sup>	TF-PhoA <sup>d-e</sup>	TF-PhoA <sup>f-g</sup>
Distance restraints <sup>a</sup>			
NOEs			
Short range (intraresidue and sequential)	858	578	615
Medium range ( $2 \leq  i-j  \leq 4$ )	257	137	211
Long range ( $ i-j  > 4$ )	781	415	587
Intermolecular	63	78	67
Hydrogen bonds	244	250	246
Dihedral angle restraints ( $\phi$ and $\psi$ )	511	480	500
Violations (mean and SD) <sup>a</sup>			
Distance restraints (Å)	0.013 +/- 0.044	0.012 +/- 0.051	0.013 +/- 0.042
Dihedral angle restraints (°)	0.04 +/- 0.44	0.04 +/- 0.37	0.07 +/- 0.50
Structural coordinates rmsd <sup>a</sup>			
PPD			
Backbone atoms	0.41 Å	0.55 Å	0.65 Å
All heavy atoms	0.70 Å	0.85 Å	0.92 Å
SBD			
Backbone atoms	1.22 Å	1.09 Å	1.22 Å
All heavy atoms	1.50 Å	1.25 Å	1.50 Å
Ramachandran plot <sup>a</sup>			
Most-favored regions	86.1%	86.4%	86.6%
Additionally allowed regions	13.7%	13.4%	13.4%
Generously allowed regions	0.2%	0.1%	0.1%
Disallowed regions	0.0%	0.0%	0.0%

<sup>a</sup>The statistics apply to the 20 lowest-energy structures of each of the three complexes. Restraints and analysis applied for the SBD and PPD parts of TF.